Supporting Information for: RNA polymerases as moving barriers to condensin loop extrusion

Hugo B. Brandão, Payel Paul, Aafke van den Berg, David Z. Rudner, Xindan Wang, Leonid A. Mirny

Contents

1 Materials and Methods **2**
1.1 Cell growth and treatment conditions . . . 2
1.2 Hi-C experiments and data processing . . . 2
1.3 ChIP-seq experiments and data processing . . . 2
1.4 Microscopy experiments and data processing . . . 3
1.5 External data sources . . . 3

2 Data processing **3**
2.1 ChIP-seq data visualization and aggregation over operons . . . 3
2.2 Hi-C data visualization . . . 4
2.3 Transcription units from predictions . . . 4

3 Models of SMC loop extrusion **4**
3.1 Calculating secondary diagonal traces from gene directions and positions . . . 4
3.2 Calculating secondary diagonal traces with "mixing" (i.e. non-independent SMC motors) . . . 6
3.3 Calculating goodness of fit for extrusion models . . . 6
3.4 Combining parameter fit surfaces (calculating global optima) . . . 7

4 Extrusion model considerations - motivation for a microscopic picture **7**
4.1 Inferring condensin's maximum translocation rate . . . 7
4.2 Estimating numbers of RNA polymerases per operon . . . 8

5 Moving barriers model **9**
5.1 Problem statement . . . 9
5.2 SMC translocation cooriented with transcription (head-to-tail interactions) . . . 9
5.3 SMC translocation opposing transcription (head-to-head interactions) . . . 10
5.4 Estimating the value of ρ, and why the optimal value varies from strain to strain . . . 12

6 Permeable moving barriers model **13**
6.1 Problem statement . . . 13
6.2 First passage times, and estimating the permeability rate μ: . . . 13
6.3 ChIP-seq profiles: SMC translocation cooriented with transcription (head-to-tail interactions) 14
6.4 ChIP-seq profiles: SMC translocation opposing transcription (head-to-head interactions) . . . 14
6.5 SMC ChIP-seq profiles: comparing head-to-head and head-to-tail encoutners . . . 15
6.6 General forms for the capture probability, $\chi_c(x)$ and the permeability rate, μ . . . 16
6.7 Simulating SMC ChIP-seq and locus crossing times . . . 17
6.8 Potential physical origins of the SMC bypass rate: implications for eukaryotic versus prokaryotic transcription . . . 18

7 Supplemental Figures **20**

8 Supplemental Tables **31**

1 Materials and Methods

1.1 Cell growth and treatment conditions

B. subtilis strains were derived from the prototrophic strain PY79 (Youngman et al. 1983), and were grown at 37°C in defined rich Casein Hydrolysate (CH) medium (Harwood and Cutting 1990). Hi-C and ChIP-seq experiments were performed for cells in mid-exponential growth phase (optical density of 0.3-0.5 at A_{600}). Transcription elongation inhibition experiments were performed with rifampicin at a concentration of 25 µg/ml for the indicated minutes.

1.2 Hi-C experiments and data processing

The high-throughput chromosome conformation capture (Hi-C) protocol was performed as described (Wang et al, 2015; Wang et al, 2017) adapted as specified from (Le et al, 2013). Briefly, cells were crosslinked with 3% formaldehyde for 30 minutes at room temperature and quenched with 125 mM glycine for 5 min, followed by a PBS buffer wash. Per Hi-C reaction, $5x10^7$ cells were used. Following cell lysis and chromatin solubilization, chromatin was digested with HindIII for 2 hours at 37°C. Digested chromatin ends were filled with Klenow and Biotin-14-dATP, dGTP, dCTP, dTTP at 25°C for 75 minutes. Products were then ligated overnight at 16°C with T4 DNA ligase. Formaldehyde crosslinking was reversed overnight in the presence of proteinase K at 65°C. The DNA was extracted twice with phenol/chloroform/isoamylalcohol (25:24:1) (PCI), precipitated with ethanol, and resuspended in QIAGEN EB buffer. Biotin from non-ligated ends was removed using T4 polymerase for 4 hours at 20°C, followed by extraction with PCI. DNA was then sheared by sonication for 12 minutes with 10 seconds on, 10 seconds off cycles, with 60% amplitude using a Qsonica Q800 water bath sonicator. Sheared DNA was used for library preparation with the NEBNext Ultra kit (E7370S) according to the manufacturer's instructions for end repair, adapter ligation, and size selection. Biotinylated DNA fragments were purified using 10 µL streptavidin beads. 5 µL of DNA-bound beads were used for PCR in a 50 µL reaction for 14 cycles. PCR products were purified using Ampure beads and sequenced using a Nextseq 500.

Paired-end sequencing reads were mapped to the genome of *B. subtilis* PY79 (NCBI Reference Sequence NC_022898.1) using the same pipeline described (Wang et al., 2015). Contact maps were generated by subdividing the 4,033,459 bp PY79 genome into 404 bins: 403 bins (starting from position 0 bp) contained mapped end reads from contiguous, non-overlapping 10,000 bp stretches of DNA; the final bin contained mapped end reads from the remaining 3,459 bp of the genome. Frequencies of binned paired-end sequence reads were normalized using the iterative correction procedure (Imakaev et al, 2013). Plotting and visualization of Hi-C contact maps were performed using Python 3.6.0 (described below).

1.3 ChIP-seq experiments and data processing

Chromatin immunoprecipitation with deep sequencing (ChIP-seq) was performed as described previously (Wang et al, 2015) and modified as specified from (Graham et al, 2014). Briefly, cells were cross-linked using 3% formaldehyde for 30 minutes at room temperature. Cells were then quenched with 125 mM glycine for 5 min, washed, and lysed as described (Graham et al, 2014). Chromosomal DNA was sheared to an average size of 200 bp by sonication using a Qsonica (Q800) water bath sonicator. After removal of cell debris by centrifugation, 50 µL of lysate was removed to serve as an "Input" control. The remaining lysate was then incubated overnight at 4°C with anti-GFP (Rudner et al., 1999) or anti-SMC (Lindow et al., 2002) antibodies and subsequently incubated by Protein A-Sepharose resin (GE HealthCare) for 1 hour at 4°C. After washes and elution, crosslinks in the immunoprecipitate were reversed with an incubation at 65°C overnight. Then, both the "Input" and "ChIP" sample DNA were treated with RNase A, Proteinase K, and extracted using PCI, resuspended in QIAGEN EB Buffer as described (Graham et al, 2014). Library

preparation was performed with the NEBNext Ultra Kit (E7370S) and sequenced using the Illumina MiSeq platform. Between 2-5 million reads were collected for each sample.

Paired-end sequencing reads from ChIP and Input samples were mapped to the genome of *B. subtilis* PY79 (NCBI Reference Sequence NC_022898.1) using CLC Genomics Workbench (CLC bio, QIAGEN). To create ChIP and Input tracks from paired-end sequence reads, a count of 1 read was added to all base pairs between the 3' and 5' positions of each mapped end (i.e. for a total of 51 counts for each of the paired end, where 51 is the number of sequenced reads from the Illumina machine). Reads that were not uniquely mappable were assigned randomly between the sites in question. In this way, we could assign reads to repetitive sequences such as the ribosomal rrn loci to give an estimate for the occupancy at those loci. For plotting, every sample was first normalized to the total number of reads. ChIP-enrichment was then calculated from the ratio of ChIP-seq signal over the Input signal (ChIP/Input). Normalization, subsequent processing and plotting of ChIP-seq data were performed using Matplotlib v2.2.2 (https://matplotlib.org/), Numpy 1.13.1 (https://www.numpy.org/) and Scipy 0.19.1 (https://www.scipy.org/) in Python 3.6.0 (https://www.python.org/).

1.4 Microscopy experiments and data processing

Fluorescence microscopy was performed using a Nikon Eclipse Ti2 microscope equipped with Plan Apo 100x/1.45NA phase contrast oil objective and an sCMOS camera. Membranes were stained with FM4-64 (N-(3-Triethylammoniumpropyl)-4-(6-(4-(Diethylamino) Phenyl) Hexatrienyl) Pyridinium Dibromide, Molecular Probes) at 3 μg/ ml. DNA was stained with DAPI (4',6-diamidino-2-phenylindole, Molecular Probes) at 2 μg/ml. Images were cropped and adjusted using MetaMorph software. Final figure preparation was performed in Adobe Illustrator.

1.5 External data sources

See Tables S1-S17.

2 Data processing

2.1 ChIP-seq data visualization and aggregation over operons

ChIP-seq data displayed in the main figures were plotted as follows. We first computed the ratio for ChIP/Input data, and then removed any "NaN" or "Inf" values; for such values, we set the number scale for these regions to 1. To display the "raw" ChIP/Input data (Fig. 5A), we used a 1-D Gaussian filter with a window size of 1 kb (using Scipy's scipy.ndimage.gaussian_filter, with sigma=1000).

Averaging of the ChIP-seq signal over genes and operons was performed by first identifying the start and end locations of each feature. Features were obtained from annotations (genome or transcription unit annotations) as in Table S1. We first classified features as cooriented or convergent with the SMC extrusion direction (i.e. head-to-head, or head-to-tail). Then, we applied the analysis separately for each of these two cases using the procedure below.

For each unique feature, we calculated its length, L, by taking the difference between the annotated start and end positions. We then defined a window of total length $3L$ centered on the feature's mid-point (i.e. L basepairs upstream, followed by the feature of length L, and L basepairs downstream), and obtained the capped ChIP/Input signal for that region. Next, we coarse-grained the signal in that region by re-binning it into 999 distinct bins (i.e. 333 bins for signal downstream, 333 bins for the feature, and 333 bins upstream); in this way, we can average the ChIP/Input signal for differently sized genes or operons.

Re-binning was done using the function zoomArray found in mirnylib/numutils.py using the default parameters (http://bitbucket.org/mirnylab/mirnylib, 2018-02-01). Briefly, it works by block-averaging the signal: Let's first define the desired final length of the array as $3L$, and the input region length as A (assuming $A \geq 3L$). Then, if A is an integer factor of $3L$, we simply coarse-grain the capped ChIP/Input signal by averaging it over consecutive, non-overlapping bins of length $\frac{A}{3L}$ (i.e. for an integer bin x of the final array, we average over bins $\frac{A}{3L}x$ to $\frac{A}{3L}(x+1)$ in the input array). In the cases where length A is not initially an integer factor of $3L$, we apply a cubic spline interpolation to the input signal such that the final length of the interpolated signal region is integer divisible by $3L$. Interpolation is performed using the scipy.ndimage.zoom

function; the applied zoom factor is the value $zoom = \lceil A/L \rceil$ (i.e. A/L rounded upwards to the nearest integer). Following interpolation of the capped ChIP/Input signal to an integer length of $3L$, we block average the signal as described above.

After coarsegraining all desired features to a final length of 999 bins, we averaged the results using the Numpy nanmean function, and plotted the results with Python's matplotlib v2.2.2.

2.2 Hi-C data visualization

All Hi-C data displayed in the paper were shown with a linear colour scale. Unless specifically indicated in the colour bar, all Hi-C contact frequencies were thresholded to a value of 0.005 to improve clarity and visibility of the secondary diagonal for display purposes. Additionally, although the most proximal 30 kb along the main diagonal of the Hi-C map was masked out for the iterative correction procedure, as is typical for bacterial and eukaryotic Hi-C data processing (Le et al., 2013; Imakaev et al, 2012), the masked-out values were filled in with the maximum of the colour scale (i.e. 0.005 or otherwise) for the purposes of display to improve the visibility of the data and avoid map rendering artefacts due to empty pixels.

We opted to display Hi-C maps with the *ori* at the center, with the main diagonal going from the bottom left to top right. As such, all contact matrices are re-centered using Numpy's roll() function separately along each dimension, and flipud(). i.e. for a contact matrix, M, and numpy imported as np, we call M = np.flipud(np.roll(np.roll(M,-shiftBy,axis=0),-shiftBy,axis=1)). Specifically for *B. subtilis* PY79, the Hi-C contact map (M) is a 404x404 numpy array and we shift/re-center the map by 202 bins (i.e. with shiftBy=202).

2.3 Transcription units from predictions

Transcription unit annotations used in this study (see Table S1) were acquired from the BioCyc database (Karp et al., 2016). First, we obtained the transcription units using the database SmartTables (Travers et al., 2013). Transcription units were computationally predicted using software previously described (Romero and Karp, 2002) for the *B. subtilis PY79* genome and others. The SmartTable was configured first to list the genes of the transcription unit, and the right- and left-end positions of those genes. SmartTables were exported to a spreadsheet, and subsequent spreadsheet manipulations/parsing were performed using Python and the Pandas v0.22.0 data analysis library (https://pandas.pydata.org/). To determine the transcription unit start and end positions, we searched for the maximum and minimum postions of all the genes in the list. The orientation of the transcribed unit was determined by the orientation of the genes within the transcription unit; if the right-end positions of the genes were greater than the left-end positions, then we called these "forward facing", otherwise, if the left-end positions were greater than the right-end positions, these were annotated as "backwards facing" operons.

3 Models of SMC loop extrusion

3.1 Calculating secondary diagonal traces from gene directions and positions

For the gene positions and directions extrusion model, we first start with computing a quantity we call the D-score; the D-score is the local gene density multiplied by the relative direction of transcription to condensin translocation. We separately compute a D-score for each genomic feature: i.e. one for operons (or genes) (D_{operon}), one for rRNA loci (D_{rRNA}), and one for tRNA loci (D_{tRNA}). We will illustrate with an example using operons (e.g. D_{operon}), but a similar procedure applies to rRNA and tRNAs annotations.

To compute D_{operon} from operon genome annotations, we first initialize an array of zeros of size equal to the genome length (in basepairs). For each operon, we obtain its start and end positions and add +1 for "forward" facing operons, or -1 for "backward" facing operons at each base pair position belonging to an operon; forwards and backwards are in reference to the linear genome coordinate and the relative translocation direction of condensin (i.e. forwards = "head-to-tail" type encounters, backwards = "head-to-head" type encounters). We apply a similar procedure for D_{tRNA} and D_{rRNA}.

We then make the D-scores mutually exclusive (i.e. non-overlapping). Since operon annotations may overlap with rRNA annotations or tRNA annotations, for each basepair (or array position), i, we set the

$D_{operon}(i) = 0$ if $D_{tRNA}(i) \neq 0$ or $D_{rRNA}(i) \neq 0$. Next, we set $D_{tRNA}(i) = 0$ if $D_{rRNA}(i) \neq 0$. This procedure is done to avoid double-counting the times to cross the loci that are multiply annotated (i.e. by operons, tRNAs and/or rRNAs).

From the D-score, we can then compute the relative locus crossing times for the clockwise and counter-clockwise directions using the parameter, γ, as defined in the main text. For each basepair (or array position), i, the traversal time is:

$$t_{clockwise,operon}(i) = max\left(-\gamma \cdot D_{operon}(i), D_{operon}(i)\right) \tag{1}$$

$$t_{counter-clockwise,operon}(i) = max\left(\gamma \cdot D_{operon}(i), -D_{operon}(i)\right), \tag{2}$$

The clockwise and counter-clockwise traversal times for condensin to cross an rRNA or tRNA feature are computed similarly; for rRNA, we replace D_{operon} with D_{rRNA} and we replace γ by ρ; for tRNA, we use D_{tRNA} and use γ as we did for operons since although these are also highly transcribed loci, it was shown that due to their short lengths, they have little effect on local genome structure (Le & Laub, 2016).

The total locus traversal time at position i (where i is defined as an index along the genome coordinate) for a particular direction of condensin translocation is evaluated as the sum of traversal times for all the features at that locus:

$$t_{clockwise}(i) = t_{clockwise,operon}(i) + t_{clockwise,rRNA}(i) + t_{clockwise,tRNA}(i) \tag{3}$$

$$t_{counter-clockwise}(i) = \sum_{\{features\}} t_{counter-clockwise,feature}(i) \tag{4}$$

The total cumulative time as a function of distance, x, from the *parS* site is the cumulative sum of Eqs.3 and 4, starting from the *parS* position (i.e. $i = parS$) :

$$T_{clockwise}(x) = \xi \cdot \sum_{i=parS}^{parS+x} t_{clockwise}(\mathrm{mod}(i, L_G)) \tag{5}$$

$$T_{counter-clockwise}(x) = \xi \cdot \sum_{i=parS-x}^{parS} t_{counter-clockwise}(\mathrm{mod}(i, L_G)) \tag{6}$$

The total genome length is L_G; mod() is the modulus function, which allows our index to run continuously along the circular genome (i.e. when the index position i reaches L_G, the genome "end", the next value is automatically $i = 1$). The calibration constant, ξ, is used to convert relative to real times (also descibed in detail in Section 4.1) and is computed using,

$$\xi_1 = \frac{L_{arm}}{v_{avg} \cdot \sum_{i=1}^{L_{arm}} t_{clockwise}(i)} \tag{7}$$

$$\xi_2 = \frac{L_G - L_{arm}}{v_{avg} \cdot \sum_{i=L_{arm}}^{L_G} t_{counter-clockwise}(i)} \tag{8}$$

and,

$$\xi = \sqrt{\xi_1 \xi_2} \tag{9}$$

$L_{arm} \approx L_G/2 \approx 2$ Mb is the length of a genome arm, and $v_{avg} \approx 50$ kb/min is the experimentally measured average rate of condensin chromosome arm juxtaposition (Wang et al., 2017). We note here that $t_{clockwise}(i)$ and $t_{counter-clockwise}(i)$ are unitless (they are relative times), therefore ξ, ξ_1 and ξ_2 have units of time.

Eqs.5-9 allows us to plot time versus distance from *parS* site graphs for each extrusion motor direction. However, to overlay the predicted trajectory of the extrusion motor pair in time on the Hi-C map, we first need distance versus time graphs (and ultimately position versus time). Thus, we first invert Eqs.5 and 6. This is done numerically by linear interpolation (using Numpy's interp function). We query a set of 10,000

time steps evenly sampled from 0 min to 50 min separately for both $t_{clockwise}(x)$ and $t_{counter-clockwise}(x)$. The interpolation results in matched pairs of spatial displacements $(x_{clockwise}(t), x_{counter-clockwise}(t))$ from the *parS* site at each of the queried time points, t. We note that $(x_{clockwise}(0), x_{counter-clockwise}(0))$=(0,0). Therefore, to plot/superimpose the predicted extrusion trajectory on the Hi-C contact map, we convert the distances into 2-D matrix positions (X,Y) using (X,Y)=$(parS + x_{clockwise}(t), parS - x_{counter-clockwise}(t))$.

3.2 Calculating secondary diagonal traces with "mixing" (i.e. non-independent SMC motors)

Unlike in the case of calculating the secondary diagonals of pairs of independently translocating SMC motors, extrusion traces cannot be easily pre-computed in the mixing model. We used the following algorithm to compute the "mixing model" trajectories. D-scores were computed as was done for in Section 3.1, and mixing times were calculated on an SMC step-by-step basis. D-scores give us the waiting time distributions for each one of the pair of SMC motors (i.e. the clock-wise and counter-clockwise moving motors).

We started the trajectory calculation by arbitrarily choosing one of the SMC motors to step forward first by one base-pair. We chose the clockwise moving motor (but this makes an unmeasurable difference for the overall trajectory at the observable distances). We define $T_{clockwise}(i)$ and $T_{counter-clockwise}(j)$ as the cumulative times for the clockwise motor and counter-clockwise motors respectively to reach genome positions i and j. We initialize these quantities as follows:

$$T_{clockwise}(i = parS) = 0$$
$$T_{conter-clockwise}(j = parS) = 0$$

We calculated the cumulative time, $T_{clockwise}$ required for the clockwise motor to reach the to take a 1 bp step using the mixing formula, where f_{mix} (which ranges from 0 to 1) is the degree to which each SMC motor is impaired by the other:

$$T_{clockwise}(i+1) = T_{clockwise}(i) + \frac{f_{mix}}{2} \cdot t_{counter-clockwise}(i) + \frac{(1-f_{mix})}{2} \cdot t_{clockwise}(j). \quad (10)$$

We also increase the position counter, i, for the clockwise motor by +1 (i.e. $i \leftarrow i+1$). In all the subsequent steps, we check whether $T_{clockwise} > T_{couner-clockwise}$ at the current positions of i and j. If so, then we update the counter-clockwise motor using:

$$T_{counter-clockwise}(j-1) = T_{couter-clockwise}(j) + \frac{f_{mix}}{2} \cdot t_{clockwise}(i) + \frac{(1-f_{mix})}{2} \cdot t_{counter-clockwise}(j), \quad (11)$$

and the counter-clockwise position index ($j \leftarrow j-1$). If not (i.e. $T_{clockwise} < T_{couner-clockwise}$), we calculate the time to take another clockwise step again using Eq. 10. This procedure is repeated iteratively until either of the motors has reached some pre-determined position or the motors have reached some maximum alloted time for the extrusion. Once $T_{counter-clockwise}$ and $T_{clockwise}$ are computed, plotting of the secondary diagonal is performed as described above.

3.3 Calculating goodness of fit for extrusion models

To evaluate the goodness of fit for values of γ and ρ in the gene position and direction model of loop extrusion, we first generated predicted traces of the secondary diagonal using the methods of Section 3.1 (and Section 3.2 for the mixing models). We queried 10^6 time-points at the interpolation step to ensure that we had sub-kilobase spatial resolution in the predicted extrusion traces. The predicted traces were returned as a list of secondary diagonal positions , i.e. (X,Y)=$(parS + x_{clockwise}(t), parS - x_{counter-clockwise}(t)))$, which we then rounded off to 10 kb resolution (to match our 10 kb binning of Hi-C maps). The rounding process resulted in many non-unique pairs of points; we filtered out the list of points to retain solely unique pairs.

Different experimental strains have different lengths of the secondary diagonal; this is due to the fact that the diagonals end roughly where condensin reaches the *ter* site, and will depend directly on the initial

position of the *parS* site. As such, we resitricted the analysis and computation of the goodness of fit of each extrusion trace to a fixed number of Hi-C bin " steps". The number of steps was fixed on a strain by strain basis, and were counted as follows: we used the same procedure outlined above with the model parameters $\gamma = 1$, $\rho = 1$. i.e. after generating the extrusion trace (sampled at 10^6evenly spaced temporal samples from 0 to 50 min), rounding the position to the nearest 10 kb bin, and filtering for unique bins; the total number of counts per strain were set equal to the number of unique (X,Y) pairs.

The goodness of fit value was computed as follows: First, to remove the dependence of contact probability decay with distance away from the main diagonal, we normalized the Hi-C contact matrix by dividing out the expected dependence on distance (i.e. we divided each diagonal parallel to the main diagonal by the mean value for that diagonal). From these "observed over expected" Hi-C maps ($M_{o/e}$), we obtained the Hi-C map score $M_{o/e}$(X,Y), and added the Hi-C scores for all values of the unique (X,Y) positions list. We divided the final sum by the number of queried values (i.e. to compute the mean).

This procedure was performed for varying γ and ρ values. To generate plots, we queried all values of ρ , γ, from 0.5 to 10 using increments of 0.5, and from 10 to 100 using increments of 5.

3.4 Combining parameter fit surfaces (calculating global optima)

To combine the experimental parameter fit (i.e. goodness of fit) surfaces, we calculated the arithmetic mean of the goodness of fit surfaces. We restricted the analysis to strains with sufficiently long secondary diagonals. This is because some strains (e.g. BWX3381 with a *parS* site at -117^o) have a very short secondary diagonal, which resulted in poor goodness of fit surfaces (i.e. large variations in parameter values did not significantly change the overall sum of Hi-C values along the extrusion trace).

4 Extrusion model considerations - motivation for a microscopic picture

4.1 Inferring condensin's maximum translocation rate

Previously, the average speed of condensin translocation has been measured *in vivo* in *B. subtilis* (Wang et al., 2017); the average speed of translocation is $v_{avg} \approx 833$ bp/s. The maximum rate of condensin extrusion (v_{max}) based on the genome annotation model is related to the average rate of extrusion (v_{avg}) by:

$$v_{avg} = \frac{v_{max}}{\frac{1}{N_{arm}} \sum_{i=1}^{N_{arm}} \eta_i}, \tag{12}$$

where N_{arm} is the number of basepairs of a genome arm, η_i is the fold-increase in time it takes condensin to cross any single basepair against the direction of the gene relative to the cooriented direction. The value of η_i is set based on the following rules:

$$\eta_i = \begin{cases} \gamma & \text{if condensin crosses a gene convergent with transcription} \\ \rho & \text{if condensin crosses an rRNA locus convergent with transcription} \\ 1 & \text{otherwise} \end{cases} \tag{13}$$

We arrive at this expression as follows. The average rate of extrusion down any single chromosome arm of length L_{arm} (which has units of length in bp), in terms of real time can be calculated through our genome annotation model up to a constant, ξ, which has dimensions of time and converts relative times per basepair (i.e. η_i) to real time:

$$L_{arm} = v_{avg} \cdot T_{avg} = v_{avg} \cdot \xi \cdot \sum_{i=1}^{N_{arm}} \eta_i \tag{14}$$

T_{avg} is the real time it takes for condensin to traverse the distance L_{arm} at the average speed, v_{avg}. The same distance L_{arm} can be traversed at the maximum rate of extrusion, v_{max} (and time T_{max} according to our assumptions for η_i above), if all the genes are cooriented with transcription (i.e. $\eta_i = 1$ for all loci):

$$L_{arm} = v_{max} \cdot T_{max} = v_{max} \cdot \xi \cdot \sum_{i=1}^{N_{arm}} \eta_i = v_{max} \cdot \xi \cdot N_{arm} \tag{15}$$

Equating the two relations, we get:

$$\begin{aligned} L_{arm} &= L_{arm} \\ v_{avg} \cdot \xi \cdot \sum_{i=1}^{N_{arm}} \eta_i &= v_{max} \cdot \xi \cdot N_{arm} \\ v_{avg} &= \frac{v_{max}}{\frac{1}{N_{arm}} \cdot \sum_{i=1}^{N_{arm}} \eta_i} \end{aligned}$$

as above. The parameters for η_i that are found to be in the best agreement with Hi-C data are: $\gamma \approx 3-5$ and $\rho = 20$. Plugging in these numbers into the relation above, using $v_{avg} = 833$ bp/s, gives the value of $v_{max} \approx 1500 \pm 200$ bp/s.

4.2 Estimating numbers of RNA polymerases per operon

In our experimental growth conditions, the bacteria divide in ~34 mins or with a doubling time of 1.7-1.8 dbl/hr. Using Fig. 2A from Klumpp and Hwa (Klumpp & Hwa, 2008), we obtain a value of ~800-1000 RNAP/cell (for actively transcribing RNA polymerases producing mRNA). Since the cells are in exponential phase, there are roughly 3.1 origins of replication per cell as previously measured (see Graham et al, 2014); thus we estimate there are roughly 2.6-3 copies of the genome per cell on average (i.e. due to multi-fork replication). This corresponds to approximately 266-333/ RNAP/genome copy. Since the genome itself is ~4 Mb long in *B. subtilis* PY79, and ~90% of the genome is covered by operons, then each operon will receive on average $(333\,RNAP)/(4000\,kb \cdot 0.9) \approx 0.09\,RNAP/kb$. This estimate of transcribing RNAP numbers is also supported by an independent observation via single-molecule studies (Golding et al., 2005). In their single molecule study, using a candidate gene of length ~4.5 kb, Golding et al. measure that the average times for a transcription burst is about 6 min, and the time between transcription bursts is roughly 37 min. In a given transcription burst, their measured average number of RNA polymerases was 2.2 RNAP/burst. This suggests that the time-average number of RNAP on a gene at any given time is $2.2 \cdot (6\text{ min}/(37\text{ min} + 6\text{ min}))/(4.5\text{ kb}) \approx 0.07$ RNAP/kb, which is close to the previously calculated number. Throughout the text use the value of ~0.1 RNAP/kb for the average number density of RNAP at regular genes.

For the case of the rRNA loci, we estimate that the RNAP density is closer to ~5-10 RNAP/kb, which we estimate with two independent ways. First, using Fig. 2A from Klumpp and Hwa (Klumpp & Hwa, 2008), we obtain a value of ~800-1000 RNAP/cell (for transcribing rRNA genes). The calculation follows closely to the one above, where we divide out the numbers of genome copies in our growth conditions, and note that rRNA genes have a total length of ~50 kb in *B. subtilis PY79*. Thus, we estimate that 266-333/ RNAP/genome copy will fall nicely into 50 kb, which results in a density of $\approx 5-6$ RNAP/kb. Next, we can obtain the relative values of RNAP at rRNA loci using our RNAP ChIP-seq data for wild-type *B. subtilis PY79*. Since the rRNA loci most heavily occupied by RNAP, we can obtain an estimate for the relative fold-enrichment of RNAP at rRNA loci compared to the rest of the genome by taking the median ChIP-seq signal for the top 50,000 RNAP ChIP-seq values, compared to the median ChIP-seq value for the rest of the genome. By our measurements, $\frac{\text{median(RNAP ChIP at rRNA)}}{\text{median(RNAP ChIP at non-rRNA)}} \approx 93$. If we set normalize the median ChIP-seq signal at non-rRNA genes such that: median(RNAP ChIP at non-rRNA)≈0.07-0.1 RNAP/kb (see paragraph above), then it follows that the median ChIP-seq signal at rRNA loci corresponds to the range 6.5-9.3 RNAP/kb, which is close to the range of values we measured by the other method. Thus, we use ~5-10 RNAP/kb as our estimate of numbers of RNAPs transcribing rRNA loci in this paper.

5 Moving barriers model

5.1 Problem statement

Let's assume that translocating RNA polymerase is an impenetrable barrier to the motion/translocation of the SMC condensin complex. The problem is to figure out the distribution of waiting times, or average time, for condensin to cross a gene body when (A) condensin translocates in the direction of transcription, and (B) when condensin translocates in the direction opposing transcription.

5.2 SMC translocation cooriented with transcription (head-to-tail interactions)

In the case of head-to-tail interactions between condensin and RNAP (Fig. 4A, left), a condensin motor subunit translocates at a high speed, v_c=1500 bp/s, on a gene (or operon) until it encounters a transcribing RNAP moving in the same direction at a much lower speed, v_r =80 bp/s. Since RNAP is assumed to be an impermeable barrier, upon RNAP/condensin encounter the condensin slows down its translocation rate to match the RNAP speed, v_r, until the end of the gene. Dissociation of RNAP allows the condensin to continue translocating at its original high speed (Fig. 4A, left).

If the condensin meets the RNAP at base position, x, then the time for condensin to cross a gene (or operon) is:

$$t = \frac{x}{v_c} + \frac{L_g - x}{v_r} \tag{16}$$

The speed of condensin, v_c, and the speed of RNAP, v_r, are assumed here to be a constant equal to their average speeds. If the probability of encountering an RNAP at any basepair position within the gene is p_e, then the total probability of a condensin encounter with RNAP at $(j+1)^{th}$ basepair is $p_e(1-p_e)^j$. We will define the length of the gene, $L_g = N \cdot l$, where N is the number of basepairs in the gene, and l =1 bp is the unit of length; equivalently, the encounter position (in units of base pairs) $x = l \cdot j$, where j is a basepair number counter which starts from the beginning of the gene. Together, these relations give the average time, $\langle t_{cooriented} \rangle$, to traverse a gene in the head-to-tail case as:

$$\langle t_{cooriented} \rangle = \sum_{j=0}^{N-1} l \cdot \left(\frac{j}{v_c} + \frac{N-j}{v_r} \right) p_e (1-p_e)^j + \frac{L_g}{v_c} (1-p_e)^N .$$

Averages are denoted by $\langle ... \rangle$. After some algebra, the above expression simplifies to:

$$\langle t_{cooriented} \rangle = \frac{L_g}{N \cdot p_e} \cdot \left(\frac{(1-p_e)\left(1-(1-p_e)^N\right)}{v_c} + \frac{(1-p_e)^{N+1} + p_e N + p_e - 1}{v_r} \right) \tag{17}$$

We can make a few simplifying approximations to clean up the expression. First, $N+1 \approx N$ Second, we use the Taylor expansion approximation $\exp(-p_e) = 1 - p_e + O(p_e^2)$, so that, $(1-p_e)^N \approx \exp(-p_e \cdot N) = \exp(-\langle R \rangle)$, where we define $\langle R \rangle = N \cdot p_e$ to be the average number of RNA polymerases on the gene. Together, these approximations give:

$$\langle t_{cooriented} \rangle \approx \frac{L_g}{\langle R \rangle} \cdot \left(\frac{\left(1 - \frac{\langle R \rangle}{N}\right)\left(1 - e^{-\langle R \rangle}\right)}{v_c} + \frac{e^{-\langle R \rangle} - 1 + \langle R \rangle}{v_r} \right) \tag{18}$$

$$\approx \frac{L_g}{v_r} - \frac{L_g}{\langle R \rangle} \left(\frac{v_c - v_r}{v_r v_c} \right) \left(1 - e^{-\langle R \rangle}\right) \tag{19}$$

$$\approx \frac{L_g}{v_c} \left(\frac{v_c}{v_r} - \frac{1}{\langle R \rangle} \left(\frac{v_c}{v_r} - 1 \right) \left(1 - e^{-\langle R \rangle}\right) \right) \tag{20}$$

The value of $\langle t_{cooriented} \rangle$ (from the unsimplified equation, Eq. 17) is plotted as a function of gene length L_g, and RNA polymerase density per kilobase ($\langle R \rangle / 1000 bp$) (Fig. 4B, left); we have assumed that

$v_c = 1500\,bp/s$ and $v_r = 100\,bp/s$ for the calculation. The value of p_e is simply the RNA polymerase density on the gene (per base-pair). Interestingly, only two parameters (the average number of RNA polymerases for that gene) and the gene length are required to calculate the time to cross the gene. Most simply, the gene length only changes the time linearly, whereas the numbers of RNAP molecules on the gene increases the time more non-trivially.

To get a better intuition for how strongly transcription affects condensin translocation rates, we plug in some real values: For a typical operon of length 3 kb in a protein-coding locus, the average RNAP density is ~0.1 RNAP/kb (or an average of 0.3 RNAP for that operon), the fold-increase in time to cross the operon (compared to the case where the condensin is moves at its maximum rate v_c) (i.e $\langle t_{cooriented} \rangle v_c / L_g$) is 2.2-fold longer, suggesting that transcription does not strongly slow down the process of condensin extrusion in the head-to-tail case. For an rRNA locus, a 3 kb operon with 5 RNAP/kb, it takes 8.2 times longer to cross the locus compared to the "free extrusion" scenario.

5.3 SMC translocation opposing transcription (head-to-head interactions)

In the case of head-to-head collisions (Fig. 4A, right), condensin translocates across a gene (or operon) at its native high speed, v_c, towards the transcription start site until it meets an RNAP. Upon encountering RNAP, condensin translocation towards the transcription start site is stopped; condensin is then pushed back to the transcription termination site by the transcribing RNAP at the speed of the RNAP transcription, v_r. Once RNAP dissociates (i.e. when it reaches the end of the gene), condensin can attempt to cross the gene again; the condensin will only successfully cross the gene if no RNAPs are encountered during its run through the gene (Fig. 4A, right).

We assume that a translocating RNAP forms a completely impermeable barrier to condensin. The time for condensin to cross a gene of length, L_g, is the sum of times for unsuccessful traversal attempts plus the time for a successful traversal.

$$\begin{aligned}
\langle t_{convergent} \rangle &= (\text{Time for successful traversal}) + (\text{Sum of times for unsuccessful traversal attempts}) \\
&= \langle t_s \rangle + \langle t_u \rangle \\
&= \langle t_s \rangle + \sum_{a=0}^{\infty} p_a \cdot \langle t_a \rangle
\end{aligned}$$

where a is the number of unsuccessful attempts, p_a is the probability of observing a unsuccessful attempts, t_a is the total time for a unsuccessful traversal attempts and t_s is the total time for a successful attempt. The sucessful traversal time is a constant:

$$\langle t_s \rangle = \frac{L_g}{v_c} \tag{21}$$

The number of attempts, A, that condensin will make before successfully traversing the gene (in the direction opposing transcription) is given by a Geometric distribution with the probability of encountering an RNAP at any position in the gene of $1 - (1 - p_e)^N$:

$$A \sim \text{Geometric}\left(1 - (1 - p_e)^N\right) \tag{22}$$

As before, N is the number of basepairs in the gene of length L_g. Since A is geometrically distributed, the probability of a unsucessful attempts to cross the gene followed by a successful attempt on the $(a+1)$th attempt is then: $p_a = \left(1 - (1 - p_e)^N\right)^a (1 - p_e)^N$. Thus, the average time for unsuccessful traversal attempts is given by:

$$\langle t_u \rangle = \sum_{a=0}^{\infty} \left(1-(1-p_e)^N\right)^a (1-p_e)^N \langle t_a \rangle \tag{23}$$

$$= \sum_{a=0}^{\infty} \left(1-(1-p_e)^N\right)^a (1-p_e)^N \cdot a \cdot \langle t_{a=1} \rangle \tag{24}$$

$$= \langle t_{a=1} \rangle \cdot \left((1-p_e)^{-N} - 1\right) \tag{25}$$

The second line follows by noting that $\langle t_a \rangle = a \cdot \langle t_{a=1} \rangle$ since the mean of the sum of a independently and identically distributed random variables is equal to sum of the means for any one variable (or a times the mean of one of the attempts).

We now seek to determine the form of $\langle t_{a=1} \rangle$. The time of a single unsuccessful traversal attempt has duration

$$t_x = \frac{x}{v_c} + \frac{x}{v_r} \tag{26}$$

assuming that a condensin meets RNAP at nucleotide position, x, in the gene. Unlike in Section 5.2, Eq. 16, where the probability of condensin encountering an RNAP was given by a simple Geometric distribution (and hence it could pass through the gene with finite probability of not encountering RNAP), in this case, we stipulate that condensin must encounter an RNAP in the gene (i.e. since the probability is conditioned to be an unsuccessful traversal attempt). Thus, x (where $x = j \cdot l$, $L_g = N \cdot l$, l =1 bp) is given by a Truncated Geometric distribution,

$$X \sim \text{TruncatedGeometric}(p_e, N)$$

$$P\left(j = \frac{x}{l}; p_e, N\right) = \frac{1}{1-(1-p_e)^N} \cdot p_e(1-p_e)^j$$

which has support $x \epsilon [0, L_g - 1]$. So, the average time for condensin to encounter an RNAP in a single attempt is related to the first moment $\langle x \rangle$

Thus,

$$\langle t_{a=1} \rangle = \left(\frac{1}{v_c} + \frac{1}{v_r}\right) \langle x \rangle$$

$$= \left(\frac{1}{v_c} + \frac{1}{v_r}\right) \sum_{j=0}^{N-1} \frac{j}{1-(1-p_e)^N} \cdot p_e(1-p_e)^j$$

$$= \left(\frac{1}{v_c} + \frac{1}{v_r}\right) \cdot \left(\frac{N}{(1-p_e)^N - 1} + \frac{1}{p_e} + N - 1\right)$$

After some calculations, Eq. 23 becomes:

$$\langle t_u \rangle = \frac{v_r + v_c}{v_r v_c} \cdot \left[\frac{(1-p_e)^{1-N} - p_e N + p_e - 1}{p_e}\right]. \tag{27}$$

Putting this together, we finally arrive at the final exact gene-crossing time (using Eqs. 21and 27):

$$\langle t_{convergent} \rangle = \frac{L_g}{v_c} + \frac{v_r + v_c}{v_r v_c} \cdot \left[\frac{(1-p_e)^{1-N} - p_e N + p_e - 1}{p_e}\right]. \tag{28}$$

With some approximations as in the previous section (i.e. $e^{-p_e} \approx 1 - p_e$, $N - 1 \approx N$, $p_e \ll 1$, and setting $\langle R \rangle \approx p_e N$), this expression becomes:

$$\langle t_{convergent} \rangle \approx \frac{L_g}{v_c} \cdot \left[1 + \frac{v_r + v_c}{v_r} \cdot \left[\frac{e^{\langle R \rangle} - \langle R \rangle - 1}{\langle R \rangle} \right] \right]. \tag{29}$$

We can plot the average times for traversal in the convergent orientation (Eq.28) as shown in Fig. 4B, on the right. Interestingly, we see that in convergent motion, average times quickly escape physiologically possible conditions as a function of RNAP density. The physiological limit we defined as the 35 minute time mark, which is the experimentally observed time to fully "zip" a chromosome arm; in reality, the limit for any single genetic feature is smaller than this value. With long loci, like ribosomal RNA loci where transcription units are close to 10 kbp long, with as few as 0.6-0.8 RNA polymerases per kilobase, we would predict that the locus would become impenetrable to condensin.

For numerical comparison with the head-to-tail interaction case we calculate $\langle t_{convergent} \rangle v_c / L_g$ (i.e. the fold-increase in time compared to the "no RNAP"/ "free-extrusion" scenario). For a typical operon of length 3 kb in a protein-coding locus, the average RNAP density is ~0.1 RNAP/kb (or an average of 0.3 RNAP for that operon), the fold-increase in time is 2.8-fold (compared to 2.2 for the head-to-tail case). This suggests that for most regularly transcribed genes, there is no strong difference in time to cross the locus in the head-to-head versus head-to-tail cases, consistent with our current results and previous results (Tran et al., 2018). In contrast, for an rRNA locus, a 3 kb operon with 5 RNAP/kb, it takes 314-fold longer to cross the locus compared to the free extrusion scenario. This 314-fold slow-down in the head-to-head scenario is in stark contrast to the 8.2-fold slow-down for the head-to-tail case. Thus, by increasing the RNAP density, there can be huge temporal penalties for crossing a locus in the head-to-head case with impermeable barriers.

5.4 Estimating the value of ρ, and why the optimal value varies from strain to strain

We can relate the value of ρ that we used in the *gene position and direction model* (Fig. 2A) to the moving barriers model derived above. The probability of crossing a gene in the "head-to-head" orientation is f_{conv} and in the "head-to-tail" orientation is f_{coord}, and the probability of crossing a locus without a gene is f_{free}; $f_{free} + f_{conv} + f_{coord} = 1$. In the *B. subtilis* genome, $f_{free} < 0.1$. Then, if one of the bidirectional extrusion motors (labelled A) is crossing a gene at genome position, x_A, and the other motor (labelled B) is crossing a different locus at position, x_B, then the instantaneous value of ρ is

$$\rho = \frac{\langle t_{convergent}\,(x_A) \rangle}{f_{free} \langle t_{free}(x_B) \rangle + f_{coord} \langle t_{cooriented}\,(x_B) \rangle + f_{conv} \langle t_{convergent}\,(x_B) \rangle} \tag{30}$$

where $\langle t_{free}(x) \rangle$ is the time to cross a locus without impediments (i.e. at the condensin motor's maximal speed). We note that it is important to use consistent "locus lengths" (e.g. the time for 1 bp, or 100 bp) to calculate each of the average quantities to obtain good estimates of ρ.

Since, as we saw above, $\langle t_{convergent} \rangle$ and $\langle t_{cooriented} \rangle$ are functions of both gene length and RNAP density (i.e. encounter probability) for the locus pair x_A and x_B, the parameter ρ that we measure from experimental fits will actually be an average quantity; the average is the weighted average over all combinations of gene lengths and RNAP densities encountered by the pair of A and B motors as extrusion occurs away from the *parS* loading site. This observation, interestingly, provides a rationale for why there are some variations in the optimal values of ρ obtained from strain to strain: as we move the *parS* site, we slightly shift the set of gene combinations (i.e. the distribution of lengths for $t_{convergent}$ and $t_{cooriented}$) encountered by the extruding motor along its path, which will result in different combinations of optimal ρ.

As a baseline minimum estimate of ρ from the moving barriers model (Fig. 4B), we note that since it measures the effect of motor A at an rRNA locus (i.e. crossing an ~10 kb operon with an RNAP density of 5-10 RNAP/kb, whereas motor B is crossing at a regular operon (~ 1-3 kb in length), with a time average density of ~0.05-0.1 RNAP/kb it follows that,

$$\begin{aligned} \rho_{moving\ barriers} &= \frac{\langle t_{convergent}\,(x_A) \rangle}{f_{free} \langle t_{free} \rangle + f_{coord} \langle t_{cooriented}\,(x_B) \rangle + f_{conv} \langle t_{convergent}\,(x_B) \rangle} \\ &> \frac{\langle t_{convergent}\,(x_A) \rangle}{\langle t_{convergent}\,(x_B) \rangle} \approx \frac{10^5 \text{ seconds}}{10 \text{ seconds}} = 10^4. \end{aligned}$$

since $\langle t_{free} \rangle < \langle t_{coordinated} \rangle < \langle t_{convergent} \rangle$.

6 Permeable moving barriers model

6.1 Problem statement

Let's assume that RNAP is a partially permeable barrier to the motion/translocation of the SMC condensin complex. Our problem is to determine the average time that SMC spends at a locus position x within a gene body due to interactions with RNAP. Assuming that the amount of time that an SMC spends at that locus is proportional to its ChIP-seq density profile, we ultimately seek to predict the SMC ChIP-seq enrichment profile as a function of RNAP density (i.e. RNAP ChIP-seq). In addition, we will derive some quantitative intuition for a potential molecular mechanism behind the slowing down of SMC when travelling head-on against genes versus in the gene direction.We will consider below the two separate cases for the SMC ChIP-seq: (A) SMC extrusion in the direction of transcription (i.e towards the transcription end site (TES)), and (B) SMC extrusion in the direction opposing transcription (i.e. towards the transcription start site (TSS)). However, before analytically estimating the shapes of the SMC ChIP-seq profiles, we will obtain estimates for the value of the rate at which condensin bypasses RNAP.

6.2 First passage times, and estimating the permeability rate μ:

The permeable moving barriers model is similar to other types of dynamical systems which have over the years garnered many different names such as: "Asymmetric Persistent Random Walks", "Markov Jump Processes", among others (Codling et al., 2008). The permeable moving barriers model can be mapped to the Telegrapher's equation, and the problem of dynamic instability of microtubules (Bicout et al., 1997).

To obtain an estimate of μ (the rate of bypassing RNAP) we turn to the calculation of the effective speed of a condensin as it traverses a locus (e.g. the rRNA genes) in the head-to-tail direction. The effective speed of traversing a gene, v_{eff}, is given by:

$$\langle v_{eff} \rangle = \frac{L_g}{T_{tot}} \tag{31}$$

where T_{tot} is the total time to cross a locus of length L_g. From Hi-C data (i.e. the length of the secondary diagonal trajectory as condensin passes the rRNA locus), we estimate that to cross 30 kb rRNA locus in the head-to-head orientation it takes about ~8-15 minutes, therefore, $L_g = 30,000$ bp, $T_{tot} \approx 480 - 900$ s, or $v_{eff} \approx 30 - 60$ bp/s.

Analogously, the problem of traversing the total length L_g can be broken into segments of "steps forward" and "steps backward". The average distance (the mean freepath) that a condensin will travel "forward" before encountering an RNAP is found as follows: We assume the condensin travels a distance d to the next RNAP in time t with speed v_c. The length of the gap, d (in the operon's frame of reference) between the condensin and RNAP shrinks from its initial (average) value of σ_{RNAP}^{-1} (the average distance between RNAPs) as RNAP moves towards the condensin at speed v_r. Thus, $d = \sigma_{RNAP}^{-1} - v_r t$, and $d = v_c t$. These two equations can be solved for t and d resulting in $t = \frac{\sigma_{RNAP}^{-1}}{v_c + v_r}$, and $d = \sigma_{RNAP}^{-1} \frac{v_c}{v_c + v_r}$. The average distance that condensin will travel "backwards" (pushed by and RNAP it encounters) is proportional to the RNAP speed and the mean bypassing time (i.e. inverse of the permeability rate): $v_r \cdot \mu^{-1}$. Thus, the operon/gene length L_g can be composed of the sum of n increments of length δL_i (where $i \epsilon [1, n]$), where the average length is $\langle \delta L_i \rangle = \sigma_{RNAP}^{-1} \cdot \frac{v_c}{v_c + v_r} - \frac{v_r}{\mu}$. Similarly to the distance increments, we can define temporal increments for each of the combined "forwards" followed by "backwards" steps as δT_i. The average $\langle \delta T_i \rangle$ is readily calculated: In the forward direction (before meeting an RNAP), condensin crosses the gap between the previous RNAP (or the TSS) in an average time equal to $\frac{1}{\sigma_{RNAP} \cdot (v_c + v_r)}$ (as calculated above). In the backwards direction, it spends the mean bypassing time, which is equal to the permeability rate via $1/\mu$. Thus, mean time per segment is: $\langle \delta T_i \rangle = \frac{1}{\sigma_{RNAP} \cdot (v_c + v_r)} + \frac{1}{\mu}$. The effective condensin speed can be approximated (to zeroth order) as :

$$\langle v_{eff} \rangle = \frac{1}{n} \sum_{i=1}^{n} \frac{\delta L_i}{\delta T_i} \approx \frac{\langle \delta L_i \rangle}{\langle \delta T_i \rangle} = \frac{\sigma_{RNAP}^{-1} \cdot \frac{v_c}{v_c + v_r} - \frac{v_r}{\mu}}{\left(\sigma_{RNAP} \cdot (v_c + v_r)\right)^{-1} + \mu^{-1}}. \tag{32}$$

We can solve this equation for μ:

$$\mu \approx \sigma_{RNAP} \frac{(v_c + v_r)\left(\langle v_{eff} \rangle + v_r\right)}{v_c - \langle v_{eff} \rangle}. \tag{33}$$

For the values of condensin speed, $v_c \approx 800$ bp/s, RNAP speed $v_r = 80$ bp/s, $\langle v_{eff} \rangle \approx 30 - 60$ bp/s, $\sigma_{RNAP} \approx 5 - 10$ RNAP/kb, we obtain an estimate of $\mu \approx 0.6 - 1.7\ s^{-1}$, which is close to the values that we obtain via simulations (see below).

6.3 ChIP-seq profiles: SMC translocation cooriented with transcription (head-to-tail interactions)

We next move to estimating the SMC ChIP-seq enrichment profiles analytically. We start with the case of head-to-tail interactions. The amount of time an SMC spends at any position x within a gene body will be proportional to the number of times it crosses the locus weighted by the speed of crossing it. Without loss of generality, let's define $\chi_c = \chi_c(x)$ as the probability that an SMC crosses locus x with the RNAP speed, $v_r = v_r(x)$ (which can be a position-dependent function). In other words, $\chi_c(x)$ is the probability that SMC is "captured"/blocked by an RNAP at x or upstream of x (i.e. before x, towards the TSS) and it passes x moving towards the TES by a speed limited by the local transcription elongation rate. The value $(1 - \chi_c(x))$ is then the probability that SMC crosses locus x with its native speed, v_c, which we will assume here is a constant in the absence of interactions with RNAP. The average amount of time an SMC spends at locus x is then given by the probability density $\sigma_{SMC-cooriented}(x)$:

$$\begin{aligned} k_{SMC}^{-1} \cdot \sigma_{SMC-cooriented}(x) &= \frac{1}{v_c}\left(1 - \chi_c(x)\right) + \frac{1}{v_r} \cdot \chi_c(x) \\ &= \frac{1}{v_c} + \left(\frac{1}{v_r} - \frac{1}{v_c}\right) \cdot \chi_c(x) \end{aligned}$$

where k_{SMC} is the rate at which an SMC arrives at the TSS. The observed SMC ChIP-seq enrichment is $k_{SMC}^{-1}\sigma_{SMC-cooriented}(x) \cdot v_c$,

$$SMC - ChIP_{cooriented}(x) = 1 + \left(\frac{v_c - v_r(x)}{v_r(x)}\right) \cdot \chi_c(x), \tag{34}$$

which has the interpretation that the ChIP-seq signal is enriched by a factor proportional to the difference of SMC to local RNAP speeds. Moreover, the ChIP-seq enrichment has amplitude proportional to the probability, χ_c, that SMC is "captured" or "blocked" by the RNAP upstream of position x. We will discuss below the general form that $\chi_c(x)$ can take, and consider specific example cases. For now, we simply note that $\chi_c(x)$ will depend on the density of RNA polymerase ($\sigma_{RNAP}(x)$), and can be related to a permeability rate, μ, which describes how likely it is for RNAP to block the SMC extrusion.

Interestly, and of note, we see that the ChIP-seq signal will depend on the position-dependent RNAP rate $v_r(x)$. Indeed, since the rate of RNAP transcription within the gene will determine the enrichment of the RNAP, it follows that the SMC ChIP-seq signal will be strongly (positively) correlated with the RNAP signal. For instance, in a gene body, wherever the RNAP ChIP-seq value increases (i.e. where $v_r(x)$ is lowest), we also expect that the SMC ChIP-seq value will increase, even while keeping χ_c constant.

6.4 ChIP-seq profiles: SMC translocation opposing transcription (head-to-head interactions)

For the case of SMC motion opposing transcription, we break up the problem into two contributions: one contribution is due to SMC moving unhindered by RNAP towards the TSS (Fig. 4A, row i), and another contribution from SMC moving towards the TES being pushed back by RNAP (Fig. 4A, rows ii-iii). For this derivation, we use the shorthand $\chi_c = \chi_c(x)$. Again, we define $\chi_c(x)$ as the probability that an SMC is "captured"/blocked by an RNAP somewhere between the position x and the TSS and then crosses the locus x with the RNAP speed on its way back through x (since it is being pushed by RNAP); we assume,

of course, that the SMC has already passed position x at least once at its native speed, v_c, moving towards the TSS from the TES direction .

The probability that the SMC passes a locus x only once is the probability that it traverses the gene and "escapes" without being captured and brought back; it is equivalent to : $(1-\chi_c)$. The probability that SMC passes locus x twice is the probability it fails to exit the gene (i.e. is captured and brought back) times the probability it successfully escapes capture : $\chi_c(1-\chi_c)$. The probability that it passes three times is $\chi_c^2(1-\chi_c)$, and so forth. Thus, the amount of time SMC spends at locus x is given by the density $\sigma_{SMC-convergent}(x)$:

$$\begin{aligned} k_{SMC}^{-1}\cdot\sigma_{SMC-convergent}(x) &= \frac{1}{v_c}\left(1\cdot(1-\chi_c)+2\cdot\chi_c(1-\chi_c)+3\cdot\chi_c^2(1-\chi_c)+...\right) \\ &+\frac{1}{v_r}\left(1\cdot\chi_c(1-\chi_c)+2\cdot\chi_c^2(1-\chi_c)+3\cdot\chi_c^3(1-\chi_c)+...\right) \end{aligned}$$

The terms involving v_c are understood to be the motion towards the TSS (unhindered by RNAP), and the terms involving v_r are understood as motion towards the TES as SMC is pushed back by RNAP at the local average RNAP speed ($v_r = v_r(x)$). Collecting these terms, and after some straight-forward algebra, we get:

$$\begin{aligned} k_{SMC}^{-1}\cdot\sigma_{SMC-convergent}(x) &= \frac{1}{v_c}\cdot\sum_{n=1}^{\infty} n\cdot\chi_c^{n-1}(1-\chi_c)+\frac{1}{v_r}\cdot\sum_{n=1}^{\infty} n\cdot\chi_c(1-\chi_c) \\ &= \frac{1}{v_c(1-\chi_c)}+\frac{\chi_c}{v_r(1-\chi_c)} \\ &= \frac{1}{v_c}+\left(\frac{1}{v_c}+\frac{1}{v_r}\right)\cdot\frac{\chi_c}{1-\chi_c} \end{aligned}$$

The observed SMC ChIP-seq enrichment is $k_{SMC}^{-1}\cdot\sigma_{SMC-convergent}(x)\cdot v_c$,

$$SMC-ChIP_{convergent}(x) = 1+\left(\frac{v_c}{v_r(x)}+1\right)\cdot\frac{\chi_c(x)}{1-\chi_c(x)}, \tag{35}$$

The final result for the SMC ChIP-seq enrichment within a gene can be interpreted as follows: it is the sum of the relative times to cross x in both the forward and reverse directions $\left(\frac{v_c}{v_r(x)}+1\right)$ (i.e. the average time spent at position x per crossing attempt), multiplied by the average number of attempts to cross the locus, $\frac{\chi_c}{1-\chi_c}$. The latter term is formally equivalent to the expectation value of a negative binomial distribution.

6.5 SMC ChIP-seq profiles: comparing head-to-head and head-to-tail encounters

Right away (following the two sections above), we see that within a gene body, we expect there to be a stronger enrichment of SMC in the head-to-head interaction case than the head-to-tail case:

$$\begin{aligned} fold-(change\ \ in\ \ enrichment) &= \frac{1-SMC-ChIP_{convergent}(x)}{1-SMC-ChIP_{cooriented}(x)} \\ &= \frac{\left(\frac{v_c}{v_r(x)}+1\right)\cdot\frac{\chi_c(x)}{1-\chi_c(x)}}{\left(\frac{v_c-v_r(x)}{v_r(x)}\right)\cdot\chi_c(x)} \\ &= \frac{v_c+v_r}{v_c-v_r}\cdot\frac{1}{1-\chi_c(x)}. \end{aligned}$$

Thus, part of the observed change in enrichment will come from a relative difference in densities (i.e. $\frac{v_c+v_r}{v_c-v_r}$) as condensin meets RNAP more frequently when it translocates opposite to transcription than with transcription. However, we expect that this value is relatively small (<1.3, even plugging in generous values for the condensin speed (v_c = 800 bp/s), and RNAP speeds (v_r = 80 bp/s)). Thus, the observed 1.6 to 2-fold change in SMC enrichment seen experimentally (i.e. $fold-(change\ in\ enrichment) \approx 2$ for a 0.1-1 kb operon (Fig. S11B, left), and $\approx$ 1.6 for a 1-2 kb operon (Fig. S11B, right)) between the head-to-head and head-to-tail cases cannot be accounted for just based on the differences in condensin speed. Indeed, experimental values suggest that:

$$\chi_c^{SS} \approx 0.2 - 0.4. \tag{36}$$

The capture probability, $\chi_c(x)$, can be linked to the permeability rate as we will show below.

6.6 General forms for the capture probability, $\chi_c(x)$ and the permeability rate, μ

To calculate $\chi_c(x)$, we must consider separately the cases of head-to-tail and head-to-head encounters between the translocating SMC motor and the RNAP. The value $\chi_c(x)$ will depend on the probability density of RNAP in a given operon at a given position, x, the length of the operon (i.e. the position x), and the permeability rate, μ. We compute $\chi_c(x)$ using a Master equation, and we consider only the case of head-to-tail encounters for simplicity. To write the Master equation (i.e. the time-evolution equation of the state $\chi_c(x)$), we consider the transitions between the two possible states. That is: (1) the state $\chi_c(x)$ where condensin is hindered by RNAP at position x, and (2) the state, $\chi_u(x) = 1 - \chi_c(x)$, where condensin is unhindered by RNAP at x. The transition rates between each state are illustrated in the figure below.

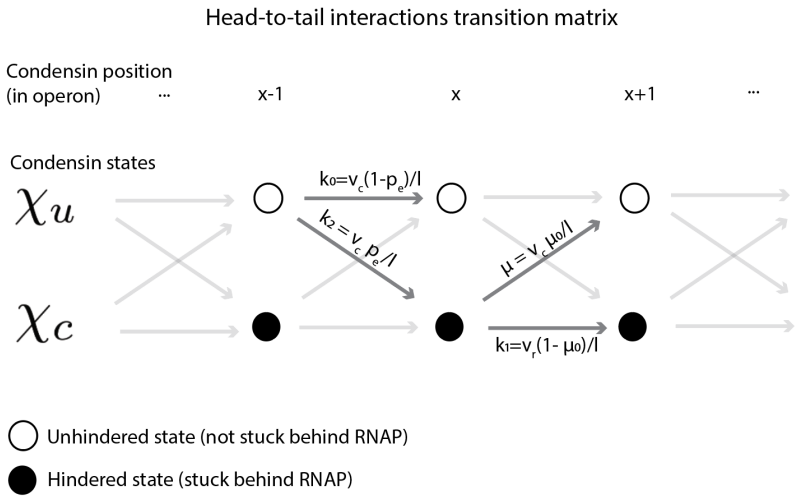

We arrive at these transition rates by considering 4 requirements. The first two requirements are for the transitions out of the state $\chi_c(x)$.

Requirement 1: The rate at which condensin bypasses an RNAP (i.e. transitions from $\chi_c(x) \rightarrow \chi_u(x+1)$) is: $\mu = v_c \cdot \mu_0/l$. We define the permeability "probability" as μ_0, so the permeability probability per basepair is μ_0/l (where l = 1 bp, as before) and μ is the value we ultimately aim to find from experiments. For simplicity, we consider only the case of constant μ_0, but in its most general form, the permeability probability could be a function of the position within an operon (i.e. $\mu_0 = \mu_0(x)$). The form of the permeability/bypass rate ($\mu = v_c \cdot \mu_0/l$) makes sense since it stipulates that the upper bound on condensin's rate of escape is its speed, v_c (i.e. when $\mu_0 = 1$).

Requirement 2: When a condensin moves from a hindered state at one position (e.g. x) to a hindered state at the next position (e.g. $x+1$) the rate is limited by the RNAP speed (i.e. v_r/l), and will also depend on condensin not escaping the bound state (i.e. $1-\mu_0$). Together, this requires the transition $\chi_c(x) \rightarrow \chi_c(x+1)$ to have a rate $k_1 = v_r(1-\mu_0)/l$. The limiting cases make sense: when $\mu_0 = 0$ (i.e. when RNAP is totally impermeable), then the transition rate becomes the RNAP speed (v_r/l) and the permeability rate becomes:$\mu = 0\ s^{-1}$ (i.e. condensin cannot bypass RNAP). On the other hand, when $\mu_0 = 1$, condensin can only step out of $\chi_c(x)$ by going back to the "unhindered" state, and it does so at the rate $\mu = v_c/l$.

The transitions out of the state $\chi_u(x-1)$ lead to the remaining 2 requirements.

Requirement 3: When an unhindered condensin takes a step, it has a probability p_e of encountering an RNAP at x. The rate of stepping from one unhindered state to the next unhindered state is therefore $k_0 = (1-p_e)\cdot v_c/l$.

Requirement 4: The rate of stepping from an unhindered state to a hindered state is $k_2 = p_e v_c$. Requirements 3 and 4 together stipulate that the total rate of condensin stepping away from the unhindered state is the total rate of stepping of an unhindered condensin, $k_2 + k_0 = v_c/l$, as required.

Thus, we arrive at the rates shown in the diagram above. We can now write down the Master equation for the time-evolution of the state, $\chi_c(x)$.

$$\frac{\partial \chi_c(x)}{\partial t} = \chi_c(x-1)\left[\frac{v_r}{l}(1-\mu_0)\right] + (1-\chi_c(x-1))\left[\frac{v_c p_e}{l}\right] - \chi_c(x)\left[\frac{v_c\mu_0}{l} + \frac{v_r(1-\mu_0)}{l}\right]. \tag{37}$$

At the steady-state, $\frac{\partial \chi_c(x)}{\partial t} = 0$. Moreover, for sufficiently large values of x, there is also a "spatial" steady-state (i.e. when $\chi_c^{SS} = \chi_c(x) = \chi_c(x-1)$). In these two conditions we obtain:

$$0 = \chi_c^{SS} v_r(1-\mu_0) + \left(1-\chi_c^{SS}\right) v_c p_e - \chi_c^{SS}\left[v_c\mu_0 + v_r(1-\mu_0)\right], \text{ or,} \tag{38}$$

$$\chi_c^{SS} = \frac{p_e}{\mu_0 + p_e}. \tag{39}$$

Finally, solving for μ_0 and recalling that $\mu = \mu_0 v_c$, we get:

$$\mu = v_c p_e\left(\frac{1}{\chi_c^{SS}} - 1\right). \tag{40}$$

We can obtain μ from χ_c^{SS} (estimated to be ~0.2-0.4 in the previous section), by noting that the average density of RNAP at non-rRNA is $\frac{p_e}{l} \approx 0.1$ RNAP/kb (see Section 4.2). Thus,

$$\mu = p_e v_c(1/\chi_c^{SS} - 1) \approx 0.12 - 0.32 \text{ s}^{-1}. \tag{41}$$

This estimate suggests that it takes up to ~8 seconds to bypass an RNAP transcribing a protein-coding gene.

6.7 Simulating SMC ChIP-seq and locus crossing times

We carried out simulations of the permeable moving barriers model to measure SMC occupancy as a function of distance within an operon and to calculate estimates of the locus crossing times. The simulations were performed on a discrete 1D lattice, with explicit RNAP and condensins. The RNAPs were mutually exclusive, and not allowed to occupy the same lattice site; similarly, condensins (if multiple were on the same operon) were mutually exclusive and could not occupy the same lattice site. Each discrete lattice site corresponded to 1 bp. Operons were simulated in the range of lengths 1 kb to 10 kb (or 1000 to 10,000 lattice sites), plus 100 lattice sites upstream and downstream of the operon. Simulations proceeded with a fixed time step equal to a condensin forward step; in this way, condensins were deterministic walkers, occupying sequential 1 bp lattice sites at a time, and the simulation time step was equal to the inverse of the condensin speed (assumed 800 bp/s, or 1.25 ms per simulation lattice site). RNAP forward steps were taken with a probability $p = 0.1$ simulation steps, corresponding to an average of 80 bp/s. RNAP were randomly initiated with exponential kinetics at the transcription start site with a probability $k_r = 10^{-3}$ to 10^{-5}, which gave rise to average numbers of RNAP per kilobase in the range of 0.1 to 10. RNAPs reaching the end of the operon (i.e. position 10,100 for a 10 kb operon) were dissociated immediately. Similarly to RNAPs, condensins were

randomly initiated with exponential rates corresponding to probability 10^{-4} per simulation time step, this corresponds roughly to 1 SMC passing through a TSS (for the first time) every 12.5 seconds or a separation of roughly ~20 kb per SMC. The starting position of SMCs, however, was always at lattice position "0". SMCs reaching the end of the simulation box (e.g. position 10,200 for a 10 kb operon) were dissociated. We estimate this is a ~ 10-fold overestimate of the density of SMCs, but we note (see below) that for the purposes of simulating SMC ChIP-seq profiles, it does not significantly change the shapes of the observed curves.

The simulation step rules proceeded as follows. If an RNAP took a tentative forward step and encountered another RNAP at the next lattice site, the step was aborted (i.e. due to the mutual exclusion). If an SMC moved a forward step and it encountered another SMC, the step was similarly aborted (due to mutual exclusion). However, if an SMC took a tentative forward step and it encountered an RNAP, it took the step with probability μ (corresponding to the rate of bypassing RNAP). Only in this situtation were two molecules allowed to occupy the same lattice site. The typical simulation was run for 10,000,000 steps. In each simulation step, all particle positions were updated according to the rules above, and the average time to cross from the transcription start site to end site were computed.

To compute the SMC enrichment profiles, we created an array of positions (equal to the length of the simulation box) and added 1 count for each unique cluster of SMCs at each time point sampled at the position closest to the RNAP. Sampling was done once per simulation time step. Unique clusters were defined as sets of contiguous lattice sites occupied by successive SMCs. For instance, consider SMC at lattice positions in the set $\{i$=15,100,101,102,5056,5057,5090$\}$. This hypothetical scenario would constitute 4 clusters of SMCs (a single SMC at position 15, a cluster of 3 SMCs registered at position 102, a cluster of 2 SMCs registered at position 5057, and a single SMC at the position 5090. Thus, similarly to ChIP-seq, which would not distinguish between clusters of adjacent SMCs (and thus does not strictly speaking measure SMC enrichment), we account for the potential confounding factor of SMCs forming a consecutive train in our simulations. We note, however, that for the experimentally relevant densities of RNAP, permeability rates, and even our overestimate of the condensin density, the average number of SMCs per operon were typically less than 2. Thus, clustering of SMCs was minimal, and this justifies using the larger SMC density (i.e. to obtain more occurrences of operon traversal). SMC enrichment was performed by dividing the counts per lattice site by the mean of the first 100 lattice sites in the simulation box (i.e. the sites before the operon).

6.8 Potential physical origins of the SMC bypass rate: implications for eukaryotic versus prokaryotic transcription

The microscopic origin of the permeability of transcription machinery to SMC translocation is unknown. We discuss and estimate here some possibly relevant microscopic details for the transactions of transcription and SMCs: The size of isolated eukaryotic RNAPs are comparable to bacterial ones (approximately 10-15 nm in diameter (Phillips and Milo, 2016)). However, sizes of whole elongating transcription complexes in eukaryotes can considerably larger. A typical 1.5 kb to 3 kb bacterial operon will transcribe RNA of physical dimensions up to ~ 60 nm x 30 nm x 10 nm (Gopal et al, 2012). The smallest cross-sectional area of such folded RNA molecules alone is 30 nm x 10 nm, which may be expected to fit through an SMC complex lumen. However, due to co-transcription and translation of bacterial operons, polysomes could substantially increase this minimum size. Electron microscopy images of elongating mRNA in E. coli show that trains of co-translating ribosomes can cluster on elongating mRNA molecules (Miller et al, 1970). Combining RNAP, mRNA, and one to three ribosomes (plus polypeptide chains), each of diameter 20-30 nm (Phillips and Milo, 2016) could result in elongating transcription complexes of physical dimensions comparable to the SMC lumen (Fig. 5D). We estimate the volume of such a co-transcription and translation complex will range from $\approx 90 - 120 \times 10^3$ nm^3, which will have a globular diameter of ~45-60 nm. With shape fluctuations on the order of 10-20% in size, this complex could be just small enough to squeeze through the SMC lumen. In comparison, the average human gene is ~27 kb (Watson et al, 2014). While eukaryotes do not have coupled transcription and translation, there is translation coupled splicing, and the spliceosome is of similar size to the ribosome (Watson et al, 2014). We estimate that the eukaryotic RNAP with its 9-fold longer pre-mRNA and spliceosomes will have a globular diameter >70 nm. Fluctuations in shape of >30% would be needed for the eukaryotic transcription complexes to fit in an SMC complex lumen. Other factors which we did not consider here such as nucleosomes (~10 nm diameter with DNA), RNA capping proteins (bound to the

RNAP) and others would be expected to further increase the steric size of the barrier occluding an SMC. If the bypass rate of SMCs depends on the size of the physical steric barriers in their path, there will likely be some important differences in the rate at which an SMC can bypass transcription machinery in prokaryotes versus eukaryotes. Further works needs to be carried out to determine how much the size of the steric barrier plays a role in the rate of SMC translocation.

7 Supplemental Figures

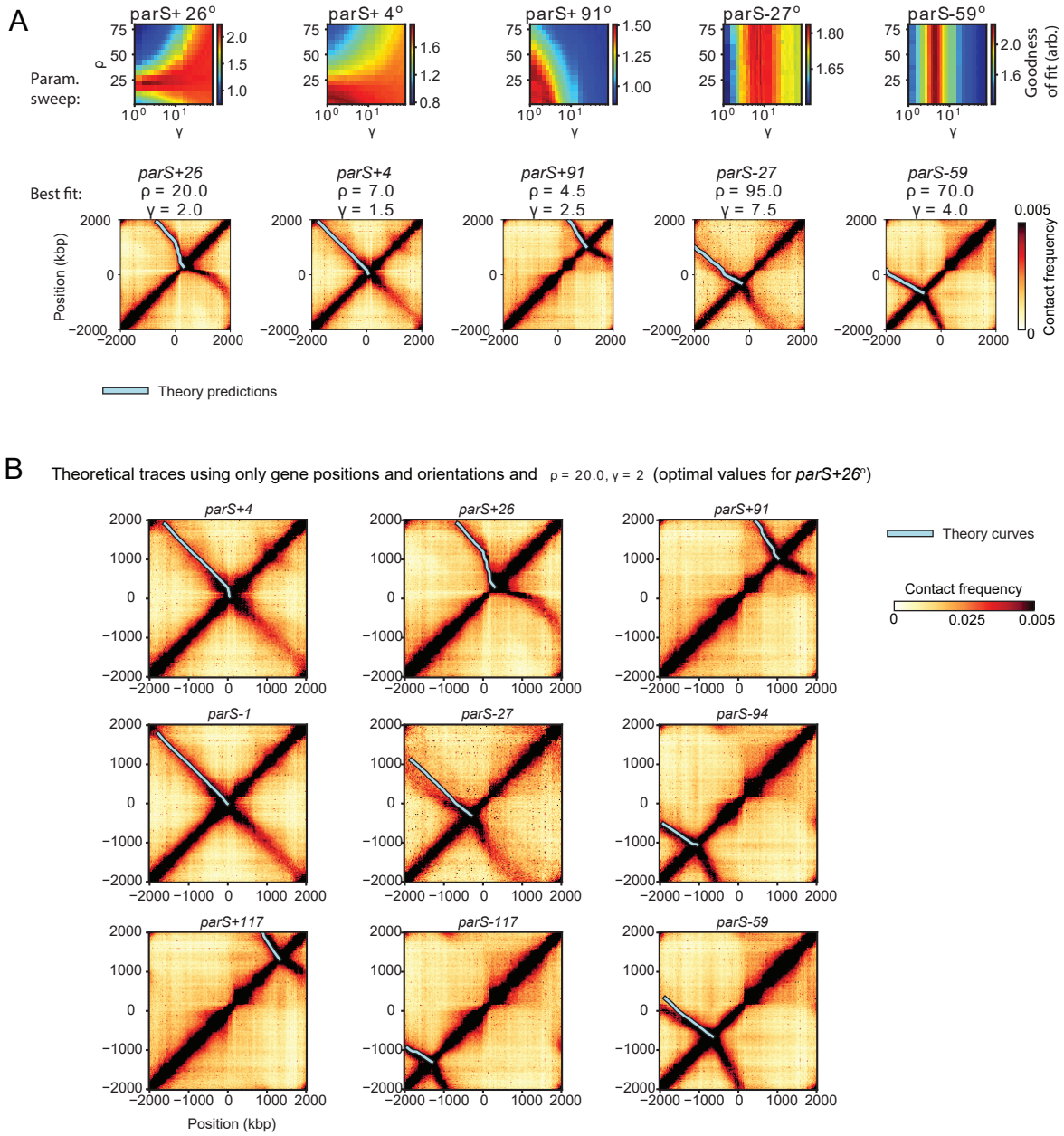

Figure S1: Strain-specific optimal parameters for the gene position and direction **SMC trajectory model.** (A) Strain-specific optimal parameter values are obtained from a parameter sweep (top), and the optimal trajectories are superimposed on the respective Hi-C maps (bottom). (B) Condensin extrusion trajectories are created using the optimum parameters (γ= 2 and $\rho = 20$) for a representative strain ($parS + 26^o$) to predict extrusion traces in 9 other strains with high fidelity.

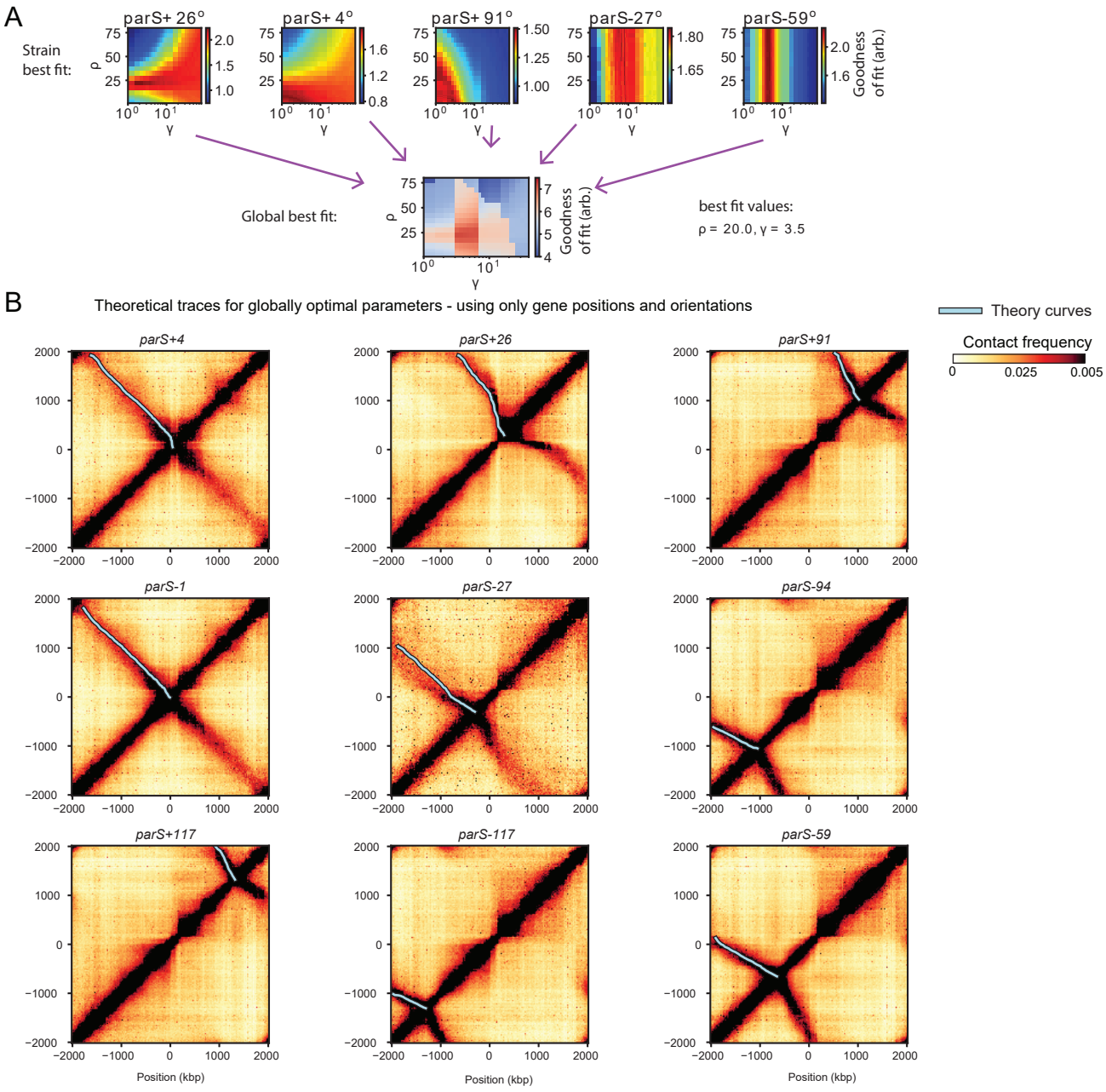

Figure S2: Obtaining globally optimal parameters for the gene position and direction SMC trajectory model. (A) Adding together strain-specific parameter goodness of fit values gives the "globally optimal" goodness of fit values (see Supporting Information for details). (B) Best-fit (globally optimal) extrusion traces plotted against each strain. The best fit value used for all traces is: $\gamma = 3.5$, $\rho = 20$ (corresponding to Fig. S2A).

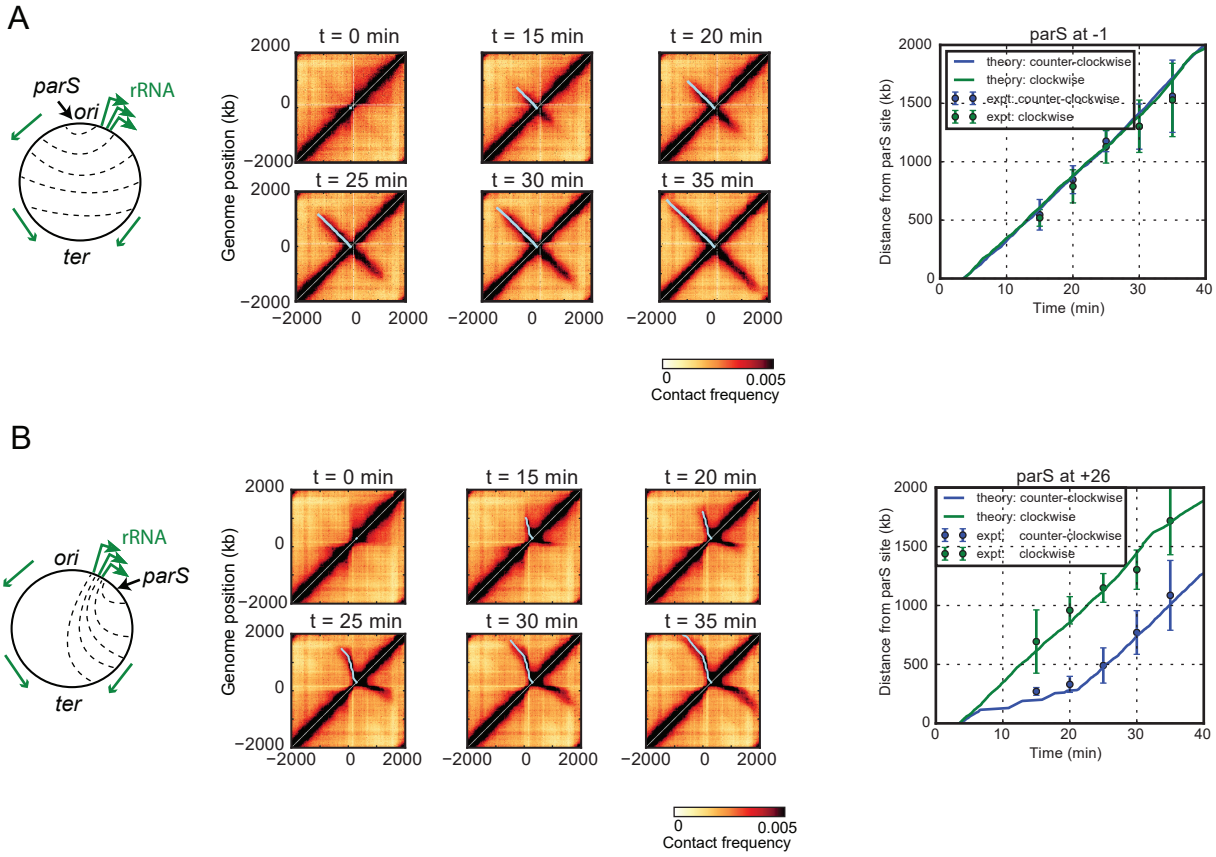

Figure S3: Comparison of gene-position and direction model of SMC translocation to time-course Hi-C data. A comparison of the predicted time-trace of extrusion to experimental data for (A) a strain with a single *parS* site at the -1^o position and (B) a strain with a single *parS* site at the $+26^o$ position. Traces were computed using v_{avg}= 50 kb/min (as measured in Wang et al., 2017), and the global optimum parameters as in Fig. S2A. The Hi-C maps show a time-course following induction of ParB (the condensin loader) at $t = 0$ min. The theoretical trace (light blue line) is superimposed on the Hi-C map. On the right, the model time-course predictions for distance of the extruding motor away from the parS site versus time are shown against measurements of extent of juxtaposition (see Wang et al., 2017); the mean and standard deviation of the measured values are displayed for comparison with the theoretical value. Note that the standard deviations do not represent true "errors" on the measurements but are shown to demonstrate the range of expected "maximum extent" values given a set of cutoff thresholds.

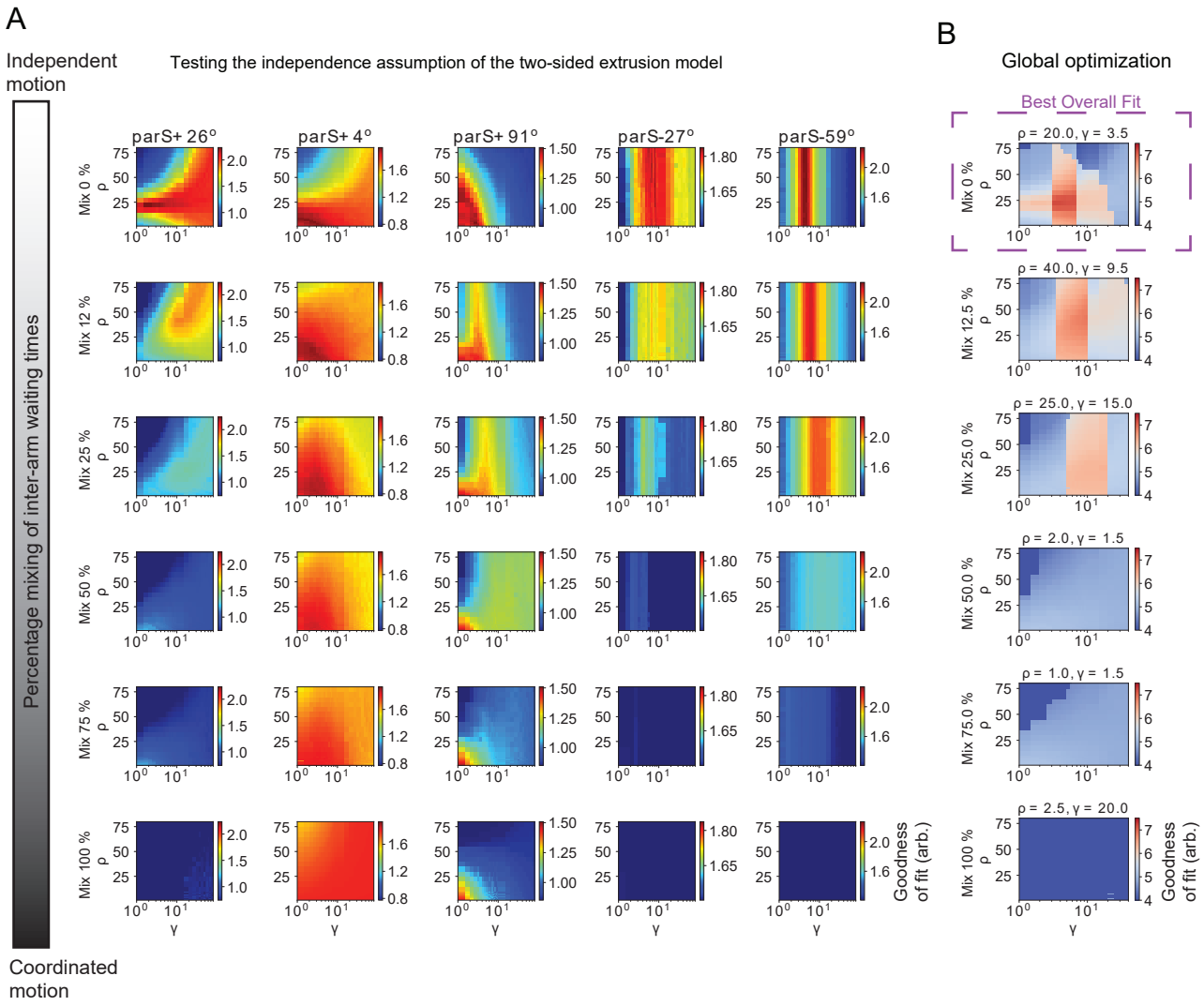

Figure S4: Testing the independence assumption of the two SMC motor activities. (A) Parameter sweep (parameters, γ, ρ) for SMC translocation trajectories calculated using the gene directions and position model with an inter-motor activity "mixing fraction". Different rows correspond to various degrees of "mixing" interactions (mixing 0% is for independently calculated trajectories of SMC away from the parS site; mixing 100% is the perfectly correlated case of identical trajectories). (B) The global optimum best fit surfaces for each mixing model calculated using the sum of best fit surfaces for each of the 5 different bacterial strains in panel A; interestingly, the overall best fit occurs for the "mixing = 0%", which contains both the overall highest, and most defined best fit values (i.e. dark red); the models' overall goodness of fit decreases progressively from the "Mix=0%" to "Mix=100%"; the overall best fit values for γ and ρ are indicated above each surface.

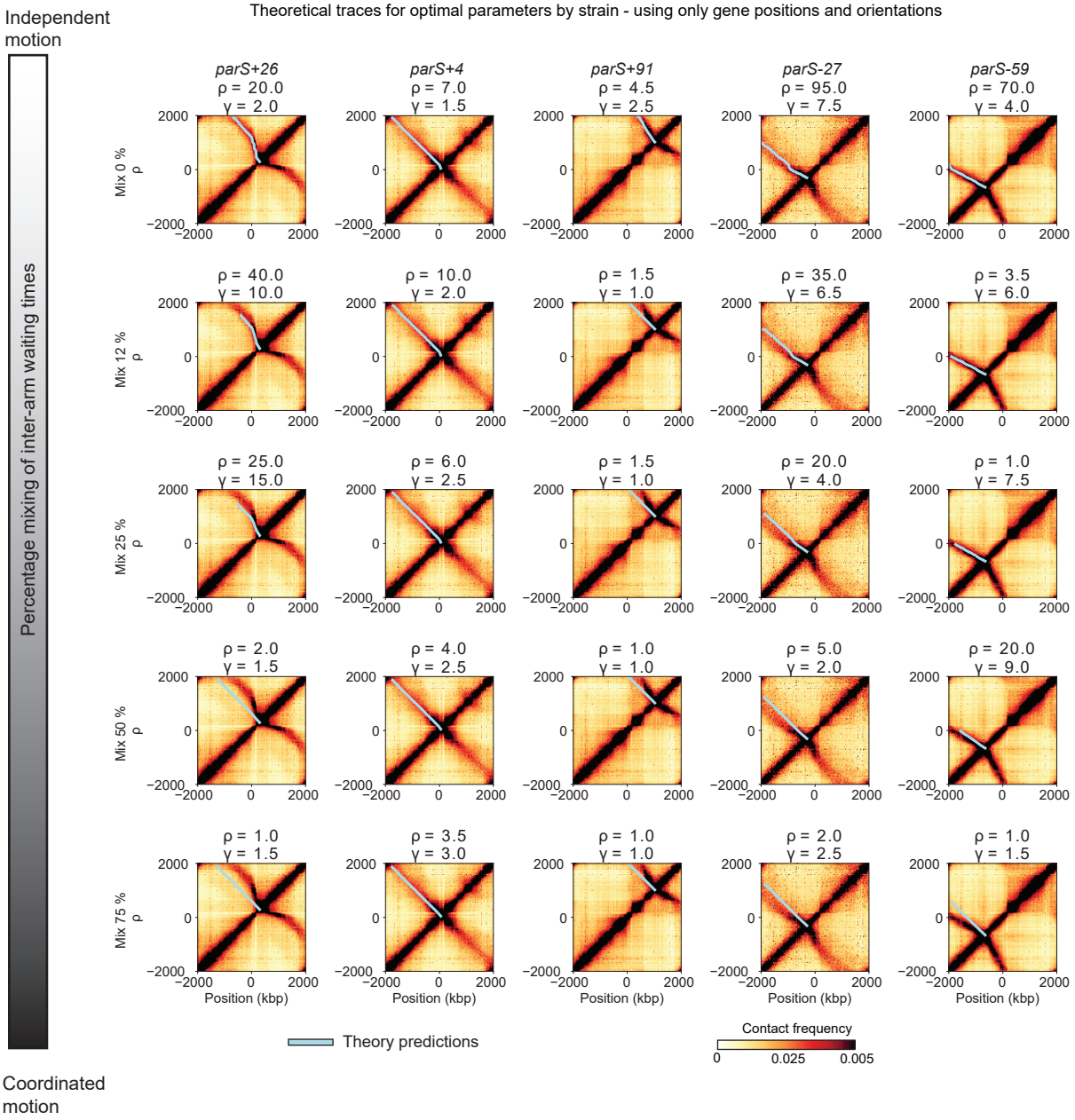

Figure S5: Best-fit (optimal by strain) extrusion traces calculated for the gene position and direction model for different mixing fractions. The best fit values of γ and ρ are indicated above each Hi-C map (corresponding to Fig. S4A panels).

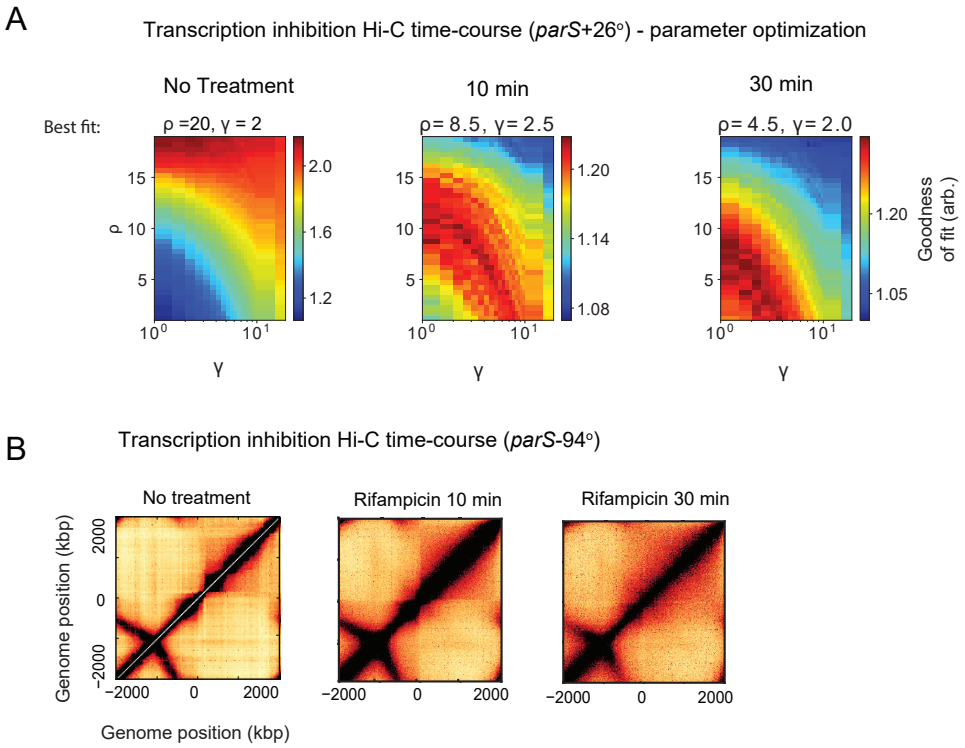

Figure S6: Time-course of transcription inhibition (rifampicin treatment) experiments. (A) Parameter sweep for SMC trajectories (gene position and orientation model), following rifampicin treatment of a strain with a *parS* site at the $+26^o$ position. Surprisingly, the optimal parameter value for γ remains largely unchanged, but ρ decreases significantly (to a level close to the global optimum value of γ) (B) Time-course following rifampicin treatment for a strain with a *parS* site at the -94^o position – no significant changes to the angle of the secondary diagonal are apparent.

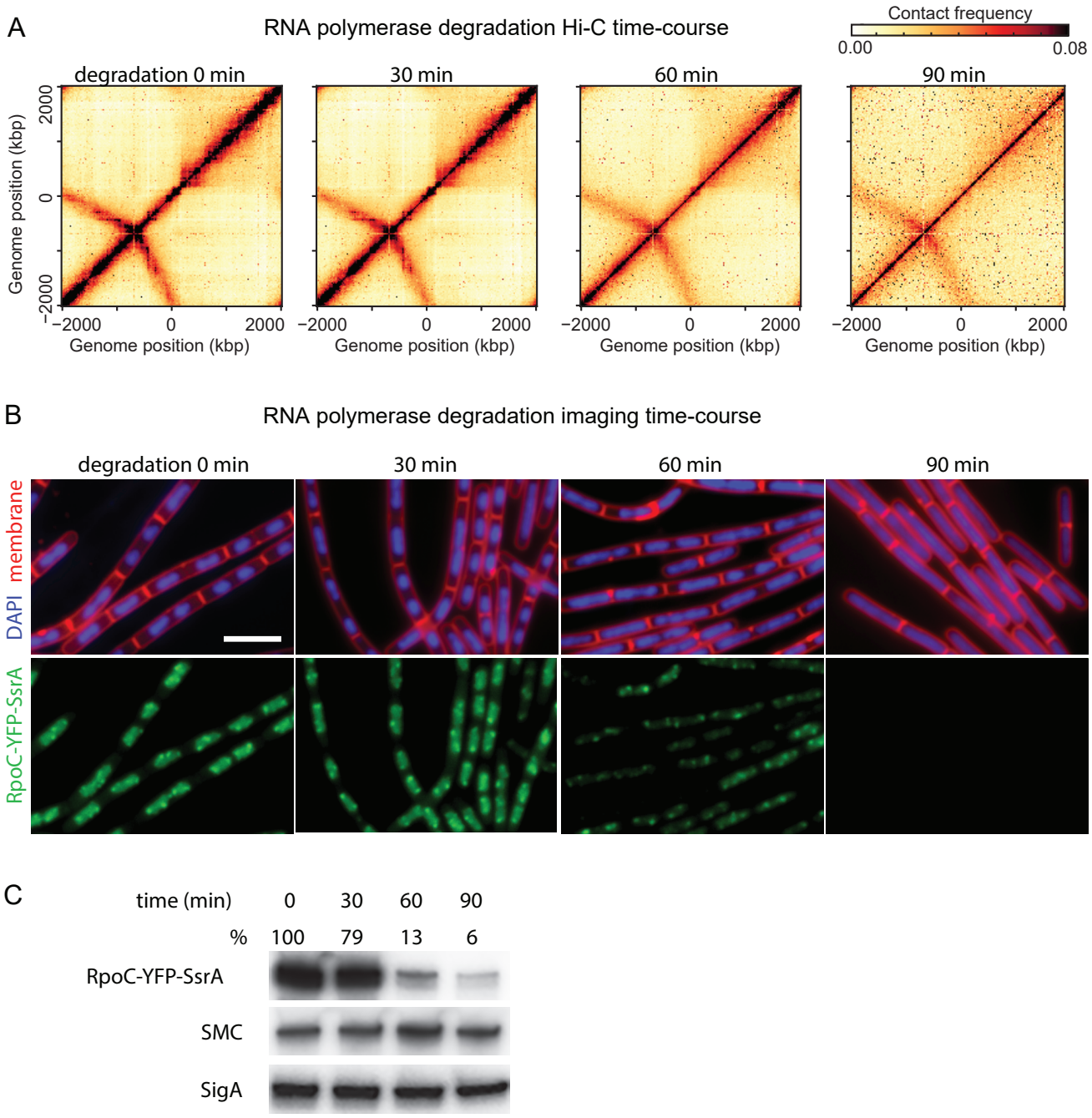

Figure S7: Effect and quantification of RpoC-YFP-SsrA degradation. (A) Time-course Hi-C following induction of RNAP (RpoC-YFP-SsrA) degradation. (B) Representative images of DAPI-stained nucleoids (blue), FM4-64-stained membrane (red), and RpoC-YFP-SsrA (green) in cells induced for RpoC-YFP-SsrA degradation for the indicated times. The YFP images were using the same scale across all different time points. Similar to rifampicin treatment (Wang et al, 2017), degradation of RpoC-YFP-SsrA caused nucleoids to fill up the whole cell. Bar, 4 µm. (C) Immunoblot analysis of RpoC-YFP-SsrA degradation. The same samples were used for Hi-C experiment in (A). GFP, SMC and SigA antibodies were used for the three panels respectively. The percentage of remaining RpoC-YFP-SsrA after degradation is indicated. Immunoblots were analyzed using ProteinSimple AlphaView software. The protein levels of SMC and SigA were largely unchanged in the time course of the experiment.

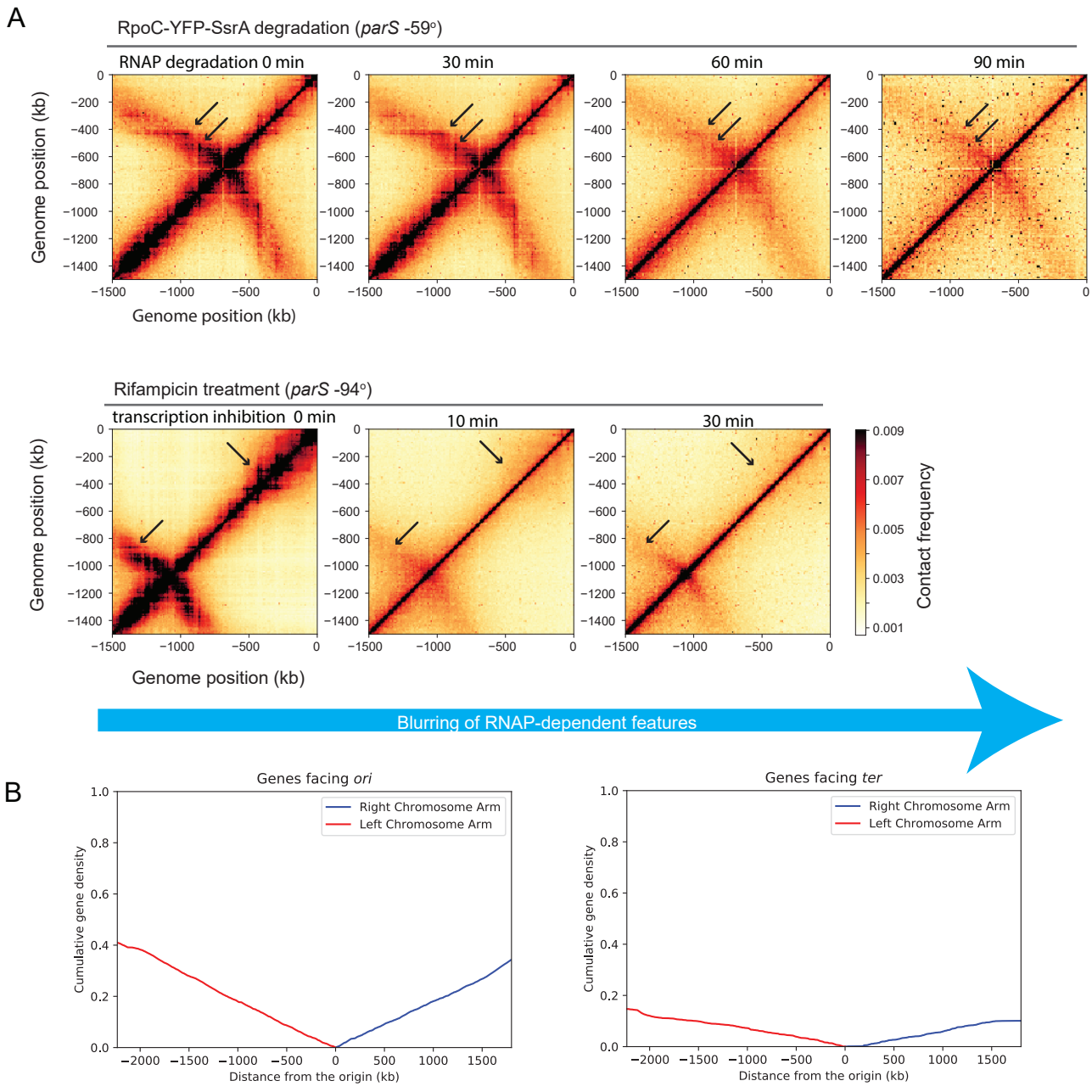

Figure S8: Transcription dependent features on Hi-C maps, and gene orientation density map. (A) "Zoomed in" portion of Hi-C map showing features (black arrows) of the Hi-C data which disappear after transcription inhibition or RNAP degradation. Specific "points" of high interaction frequency on the secondary diagonal often co-localize with highly transcribed genes. Features ("X"-shapes and "stripes") on the primary diagonal largely also disappear in the absence of RNAP or transcription. (B) Cumulative density of genes pointing towards the ori or ter as a function of distance from the ori. The uniform increase of the cumulative density demonstrates that the 75% ori¬ to ter bias in gene directions is largely homogeneous throughout the genome.

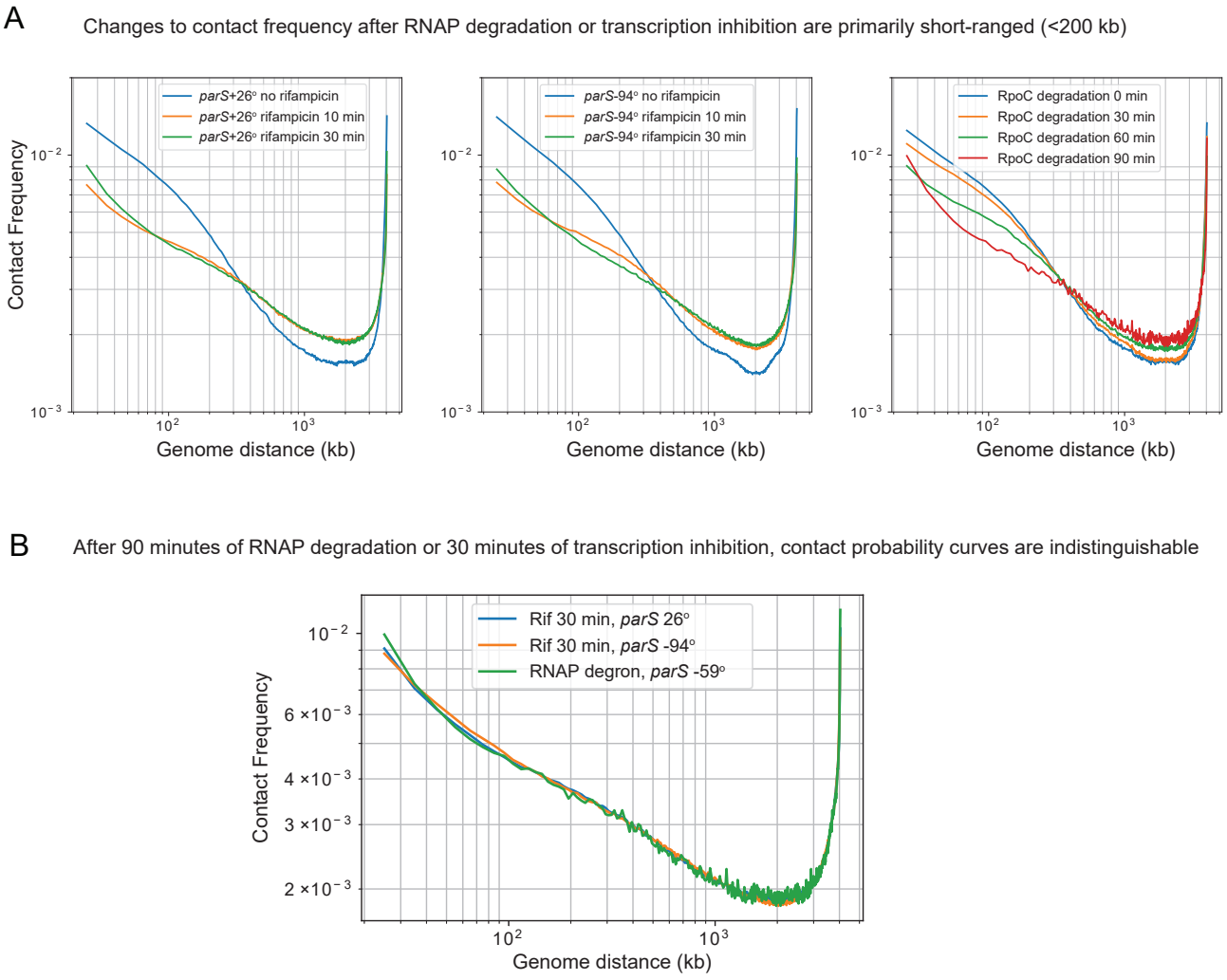

Figure S9: Comparing contact probability curves. (A) A comparison of Hi-C interaction frequencies versus genomic distance between pairs of loci in 3 different strains over a time-course of Hi-C data of rifampicin or RNAP degraded cells. (B) After rifampicin treatment (30 min) or RNAP degradation (90 min) contact probabilities of 3 different strains become indistinguishable from each other; this suggests that both RNAP degradation and transcription inhibition by rifampicin have similar effects on short-range chromosome contacts (<200 kb).

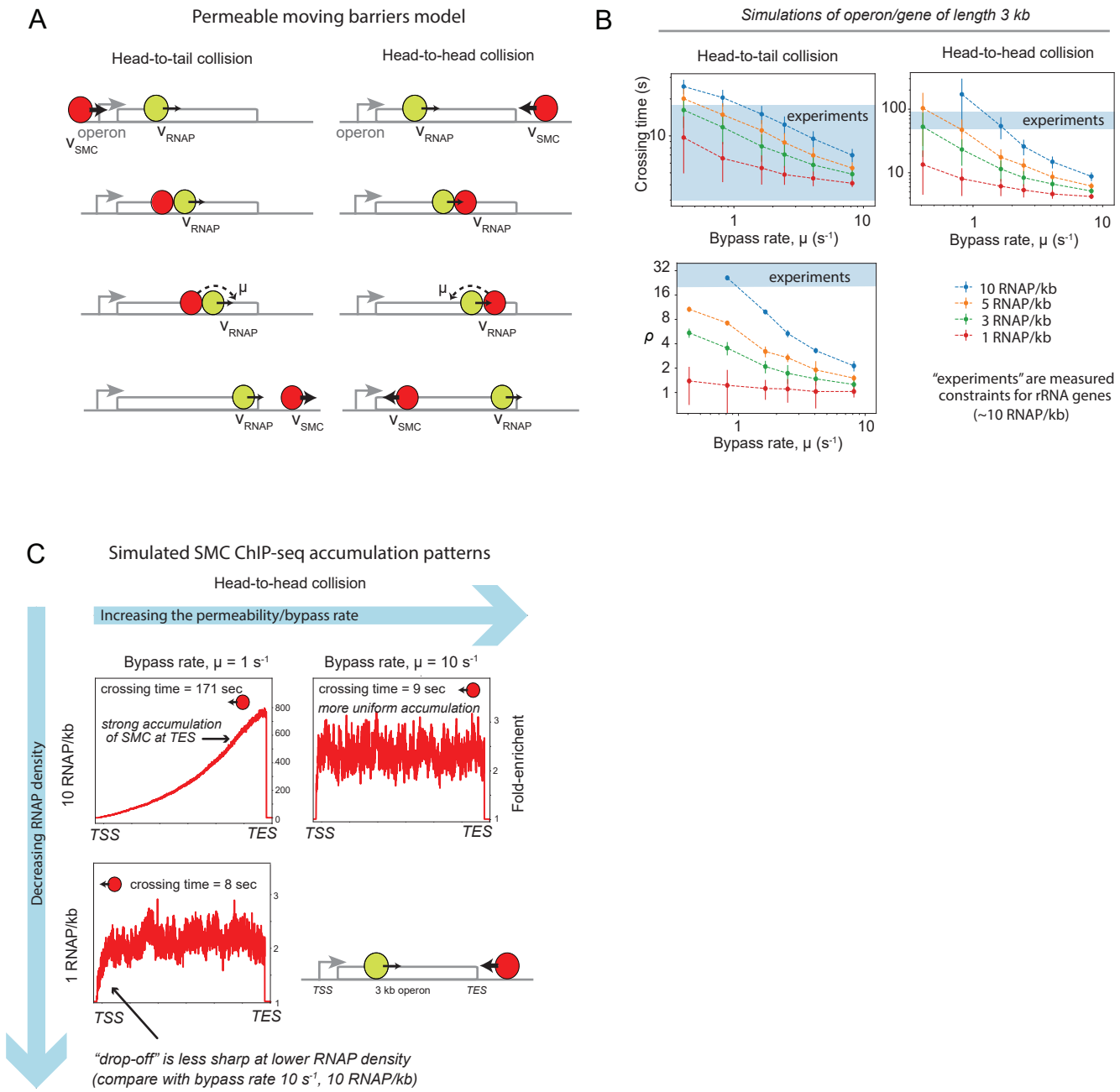

Figure S10: Permeable Moving Barriers Model. (A) Schematic illustration showing the moving barriers model with permeable barriers for both the cases of head-to-head and head-to-tail SMC/RNAP interactions. (B) Simulations of the times to cross the gene in the head-to-head and head-to-tail cases for a range of RNAP densities on a 3 kb gene. The blue line shows the experimentally inferred range of times to cross an rRNA gene of length 3 kb. From the head-to-head and head-to-tail times, the parameter ρ is also estimated (see Supporting Information); interestingly, the simulations suggest that for rRNA genes, condensins must be able to bypass RNAP at rates between $0.8\,s^{-1}$ and $1.6\,s^{-1}$. (C) Simulated SMC accumulation patterns within genes bodies for varying RNAP densities and permeability rates. For RNAP densities and rates below a critical value, the accumulation of SMC is uniform within gene bodies, where transcription end sites are labelled TES and transcription start sites as TSS. In cases of RNAP densities and permeability rates above the critical value, a strong accumulation of SMC is observed at the transcription end sites.

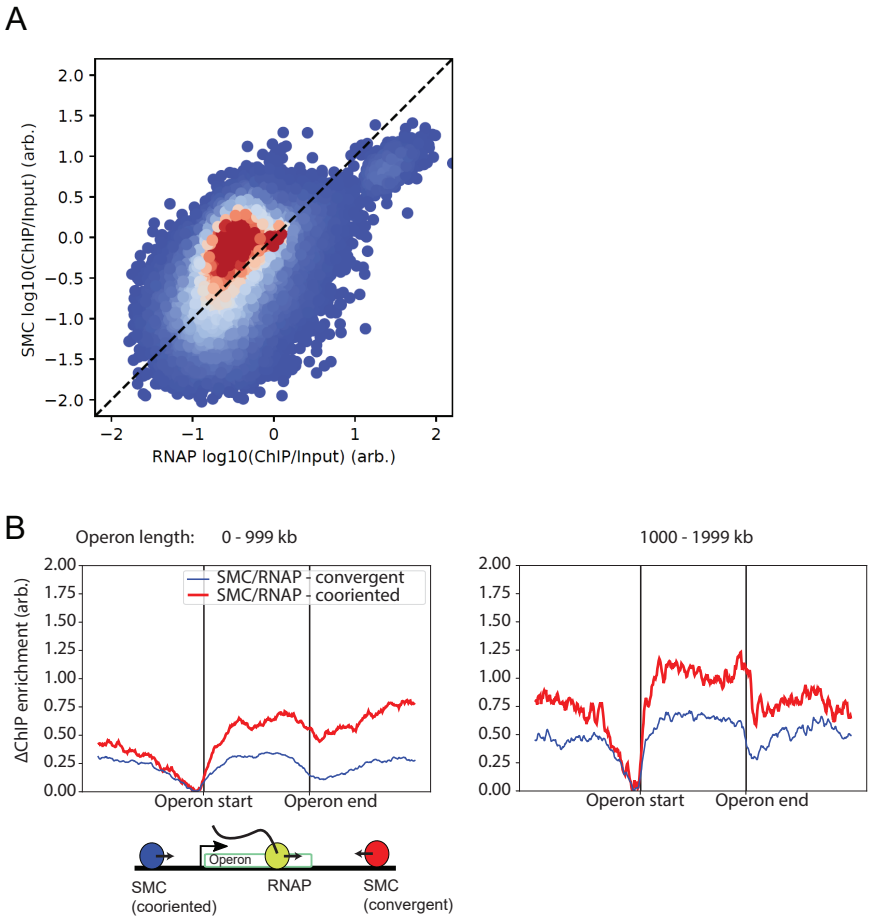

Figure S11: Experimental evidence supporting the moving barriers with permeability model. (A) SMC ChIP-seq data plotted against RNAP (RpoC-GFP) ChIP-seq data for the same strain show strong positive correlation between the two values (Pearson correlation R = 0.51, p < 10^{-28}). (B) Difference in ChIP-seq enrichment above unity for SMC tracks normalized by RNAP tracks.

8 Supplemental Tables: Data Sources

Table S1: Genome assembly and annotations

Organism	Usage	Type	Database	Source(s)
Bacillus subtilis, PY79	Hi-C, ChIP-seq mapping	Genome assembly	NCBI Reference Sequence NC_022898	Schroeder and Simmons, 2013
Bacillus subtilis, PY79	Extrusion models, ChIP-seq aggregate analysis	Gene annotations	NCBI Reference Sequence NC_022898	Schroeder and Simmons, 2013
Bacillus subtilis, PY79	Extrusion models, ChIP-seq aggregate analysis	Transcription unit annotations	BioCyc/ BioSubCyc	Karp et al, 2016; Travers et al., 2013; Romero and Karp, 2002

Table S2: Sources of Hi-C data for Fig. 1

Figure	Strain	Type	Source
Figure 1A	PY79 Wild-type	Hi-C	Wang et al., 2015
Figure 1B	BWX3221 (*parS* -94◦)	Hi-C	Wang et al., 2015

Table S3: Sources of Hi-C data and extrusion traces for Fig. 2

Figure element	Strain	Type	Source
Figure 2B	BWX3403 (*parS* +26°)	Hi-C	Wang et al., 2017
Figure 2C (top left)	BDR2985 (*parS* +4°)	Hi-C	Wang et al., 2015
Figure 2C (top center)	BWX3268 (*parS* -27°)	Hi-C	Wang et al., 2017
Figure 2C (top right)	BNS1657 (*parS* +91°)	Hi-C	Wang et al., 2015
Figure 2C (bottom left)	BWX3381 (*parS* -117°)	Hi-C	Wang et al., 2017
Figure 2C (bottom center)	BWX3221 (*parS* -94°)	Hi-C	Wang et al., 2015
Figure 2C (bottom right)	BWX3377 (*parS* -59°)	Hi-C	Wang et al., 2017
Figure 2D	BWX3403 (*parS* +26°)	Hi-C	Wang et al., 2017
Figure 2B,2C, 2D	All strains	Extrusion traces	Transcription unit annotations (Table S1); Calculations (Supplement, Section 3.1)

Table S4: Sources of Hi-C data and extrusion traces for Fig. 3

Figure element	Strain	Type	Treatment	Source
Figure 3A (*parS* +26°, left)	BWX3403	Hi-C	No treatment	Wang et al., 2017
Figure 3A (*parS* +26° right)	BWX3403	Hi-C	Rifampicin 25ug 30 min	Wang et al., 2017
Figure 3B (*parS* -94° left)	BWX3270	Hi-C	No treatment	Wang et al., 2017
Figure 3B (*parS* -94° right)	BWX3270	Hi-C	Rifampicin 25ug 30 min	This work
Figure 3 (all panels)	All strains	Extrusion traces	All treatments	Transcription unit annotations (Table S1); Calculations (Supplement, Section 3.1)

Table S5: Sources of data and calculations for Fig. 4

Figure element	Type	Source
Figure 4B	Head-to-tail calculation (no bypassing of RNAP)	This work (Supplement, Section 5)
Figure 4B	Head-to-head calculation (no bypassing of RNAP)	This work (Supplement, Section 5)
Figure 4C (right panel)	Simulations of permeable moving barrier mechanism	This work (Supplement, Section 6)

Table S6: Sources of ChIP-seq data and calculations for Fig. 5

Figure	Strain	Type	Source
Figure 5A, 5B (RpoC-GFP)	PY79 Wild-type	ChIP-seq tracks (anti-GFP)	Wang et al., 2017
Figure 5A, 5B (SMC)	PY79 Wild-type	ChIP-seq tracks (anti-SMC)	Wang et al., 2017
Figure 5B	PY79 Wild-type	ChIP-seq aggregate analysis	Transcription unit annotations (Table S1); Calculations (Supplement Section 2.1)
Figure 5C	-	Simulations: permeable moving barriers model	This work (Supplement Section 6.6)

Table S7: Source of Hi-C data and calculations for Figs. S1A, S2A

Figure	Strain	Type	Source
Figure S1A, S2A (column 1)	BWX3403 (*parS* +26°)	Hi-C	Wang et al., 2017
Figure S1A, S2A (column 2)	BDR2985 (*parS* +4°)	Hi-C	Wang et al., 2015
Figure S1A, S2A (column 3)	BNS1657 (*parS* +91°)	Hi-C	Wang et al., 2015
Figure S1A, S2A (column 4)	BWX3268 (*parS* -27°)	Hi-C	Wang et al., 2017
Figure S1A, S2A (column 5)	BWX3377 (*parS* -59°)	Hi-C	Wang et al., 2017

Figure S1A, S2A (all plots)	All above strains	Extrusion traces/ Strain goodness of fit	Transcription unit annotations (Table S1); Extrusion traces (Supplement, Section 3.1); Goodness of fit calculations (Supplement, Section 3.3)
Figure S2A (bottom plot)	All above strains	Global goodness of fit	Combining parameter fits (Supplement, Section 3.4)

Table S8: Source of Hi-C data and calculations for Fig. S1B, Fig. S2B

Figure	**Strain**	**Type**	**Source**
Figure S1B, S2B (top left)	BDR2985 (*parS* +4°)	Hi-C	Wang et al., 2015
Figure S1B, S2B (top center)	BWX3403 (*parS* +26°)	Hi-C	Wang et al., 2017
Figure S1B, S2B (top right)	BNS1657 (*parS* +91°)	Hi-C	Wang et al., 2015
Figure S1B, S2B (middle left)	BDR2996 (*parS* -1°)	Hi-C	Wang et al., 2015
Figure S1B, S2B (middle center)	BWX3268 (*parS* -27°)	Hi-C	Wang et al., 2017
Figure S1B, S2B (middle right)	BWX3221 (*parS* -94°)	Hi-C	Wang et al., 2015
Figure S1B, S2B (bottom left)	(*parS* +117°)	Hi-C	Wang et al., 2017
Figure S1B, S2B (bottom center)	BWX3381 (*parS*-117°)	Hi-C	Wang et al., 2017
Figure S1B, S2B (bottom right)	BWX3377 (*parS* -59°)	Hi-C	Wang et al., 2017
All panels	All strains	Extrusion traces	Transcription unit annotations (Table S1); Calculations for extrusion traces (Supplement, Section 3.1)

Table S9: Source of Hi-C data and extrusion traces for Fig. S3

Figure element	Strain	Type	Source
Figure S3A	BWX3352 (*parS* -1°)	Hi-C	Wang et al., 2017
Figure S3B	BWX3403 (*parS* +26°)	Hi-C	Wang et al., 2017
Figure S3A, S3B	All strains	Extrusion traces	Transcription unit annotations (Table S1); Calculations (Supplement, Section 3.1)

Table S10: Source of data and calculations for Fig. S4

Figure	Strain	Type	Calculation; Data source
Figure S4A (column 1)	BWX3403 (*parS* +26°)	Goodness of fit	This work (Supplement, Section 3.3); Wang et al., 2017
Figure S4A (column 2)	BDR2985 (*parS* +4°)	Goodness of fit	This work (Supplement, Section 3.3); Wang et al., 2015
Figure S4A (column 3)	BNS1657 (*parS* +91°)	Goodness of fit	This work (Supplement, Section 3.3); Wang et al., 2015
Figure S4A (column 4)	BWX3268 (*parS* -27°)	Goodness of fit	This work (Supplement, Section 3.3); Wang et al., 2017
Figure S4A (column 5)	BWX3377 (*parS* -59°)	Goodness of fit	This work (Supplement, Section 3.3); Wang et al., 2017
Figure S4B	All above strains	Global goodness of fit	Combining parameter fits (Supplement, Section 3.4)

Table S11: Source of Hi-C data for Fig. S5

Figure	Strain	Type	Source
Figure S5 (column 1)	BWX3403 (*parS* +26°)	Hi-C	Wang et al., 2017
Figure S5 (column 2)	BDR2985 (*parS* +4°)	Hi-C	Wang et al., 2015
Figure S5 (column 3)	BNS1657 (*parS* +91°)	Hi-C	Wang et al., 2015
Figure S5 (column 4)	BWX3268 (*parS* -27°)	Hi-C	Wang et al., 2017
Figure S5 (column 5)	BWX3377 (*parS* -59°)	Hi-C	Wang et al., 2017
Figure S5 (all plots)	All above strains	Extrusion traces	Transcription unit annotations (Table S1); Mixing model traces (Supplement, Section 3.2)

Table S12: Source of Hi-C data and calculations for Fig. S6

Figure element	Strain	Type	Treatment	Calculation; data source
Figure S6A (left)	BWX3403 (*parS* +26°)	Goodness of fit/ Hi-C	No treatment	Supplement, Section 3.4; Wang et al., 2017
Figure S6A (center)	BWX3403 (*parS* +26°)	Goodness of fit/ Hi-C	Rifampicin 25ug/uL for 10 min	Supplement, Section 3.4; Wang et al., 2017
Figure S6A (right)	BWX3403 (*parS* +26°)	Goodness of fit/ Hi-C	Rifampicin 25ug/uL for 30 min	Supplement, Section 3.4; Wang et al., 2017
Figure S6B (left)	BWX3270 (*parS* -94°)	Hi-C	No treatment	Wang et al., 2017
Figure S6B (center)	BWX3270 (*parS* -94°)	Hi-C	Rifampicin 25ug/uL for 10 min	This work
Figure S6B (right)	BWX3270 (*parS* -94°)	Hi-C	Rifampicin 25ug/uL for 30 min	This work

Table S13: Source of data for Fig. S7

Figure element	Strain	Type	Treatment	Source
Figure S7A	BWX4921 (*parS* -59º)	Hi-C	RpoC-YFP-SsrA degradation	This work
Figure S7B	BWX4921 (*parS* -59º)	Microscopy	RpoC-YFP-SsrA degradation	This work

Table S14: Source of Hi-C data for Fig. S8

Figure	Strain	Type	Treatment	Source
Figure S8A (top row)	BWX4921 (*parS* -59º)	Hi-C	RpoC-YFP-SsrA degradation	This work
Figure S8A (bottom row)	BWX3270 (*parS* -94º)	Hi-C	Rifampicin 25 ug/uL	Wang et al., 2017; This work
Figure S8B	All strains	Gene density and relative orientation	-	Transcription unit annotations (Table S1)

Table S15: Source of Hi-C data for Fig. S9

Figure	Strain	Type	Treatment	Source
Figure S9A (left)	BWX3403 (*parS* +26°)	Contact probability	Rifampicin 25 ug/uL	Wang et al., 2017
Figure S8A (center)	BWX3270 (*parS* -94°)	Contact probability	Rifampicin 25 ug/uL	Wang et al., 2017; This work
Figure S9A (right)	BWX4921 (*parS* -59°)	Contact probability	RpoC-YFP-SsrA degradation	This work
Figure S9B	As above	Contact probability	As above	As above

Table S16: Source of calculations for Fig. S10

Figure element	Type	Source
Figure S10B	Locus crossing time calculations	This work (Supplement, Section 6.4)
Figure S10B	Estimation of parameter ρ	This work (Supplement, Section 6.4)
Figure S10C	SMC ChIP-seq simulations	This work (Supplement, Section 6.4)

Table S17: Source of ChIP-seq data for Fig. S11

Figure	Strain	Type	Source
Figure S11A (RpoC-GFP)	PY79 Wild-type	ChIP-seq tracks (anti-GFP)	Wang et al., 2017
Figure S11A (SMC)	PY79 Wild-type	ChIP-seq tracks (anti-SMC)	Wang et al., 2017
Figure S11B	PY79 Wild-type	ChIP-seq aggregate analysis	Transcription unit annotations (Table S1); Calculations (Supplement Section 2.1)

References

[1] Bicout, D. J. (1997). Green's functions and first passage time distributions for dynamic instability of microtubules. Physical Review E, 56(6), 6656.

[2] Codling, E. A., Plank, M. J., & Benhamou, S. (2008). Random walk models in biology. Journal of the Royal Society Interface, 5(25), 813-834.

[3] Golding, I., Paulsson, J., Zawilski, S. M., & Cox, E. C. (2005). Real-time kinetics of gene activity in individual bacteria. Cell, 123(6), 1025-1036.

[4] Gopal, A., Zhou, Z. H., Knobler, C. M., & Gelbart, W. M. (2012). Visualizing large RNA molecules in solution. RNA, 18(2), 284-299.

[5] Graham, T. G., Wang, X., Song, D., Etson, C. M., van Oijen, A. M., Rudner, D. Z., & Loparo, J. J. (2014). ParB spreading requires DNA bridging. Genes & development. 28: 1228–1238.

[6] Karp, P. D., Latendresse, M., Paley, S. M., Krummenacker, M., Ong, Q. D., Billington, R., ... & Spaulding, A. (2015). Pathway Tools version 19.0 update: software for pathway/genome informatics and systems biology. Briefings in bioinformatics, 17(5), 877-890.

[7] Klumpp, S., & Hwa, T. (2008). Growth-rate-dependent partitioning of RNA polymerases in bacteria. Proceedings of the National Academy of Sciences, 105(51), 20245-20250.

[8] Le, T. B., Imakaev, M. V., Mirny, L. A., & Laub, M. T. (2013). High-resolution mapping of the spatial organization of a bacterial chromosome. Science, 342(6159), 731-734.

[9] Lindow, J. C., Kuwano, M., Moriya, S., & Grossman, A. D. (2002). Subcellular localization of the Bacillus subtilis structural maintenance of chromosomes (SMC) protein. Molecular microbiology, 46(4), 997-1009.

[10] Harwood, C. R., & Cutting, S. M. (1990). Molecular biological methods for Bacillus. Wiley.

[11] Imakaev, M., Fudenberg, G., McCord, R. P., Naumova, N., Goloborodko, A., Lajoie, B. R., ... & Mirny, L. A. (2012). Iterative correction of Hi-C data reveals hallmarks of chromosome organization. Nature methods, 9(10), 999.

[12] Miller Jr, O. L., & Hamkalo, B. A. (1972). Visualization of RNA synthesis on chromosomes. In International Review of Cytology (Vol. 33, pp. 1-25). Academic Press.

[13] Milo, R., Phillips, R. Cell Biology by the Numbers (Garland Science, Taylor & Francis Group, LLC, 2016). pp.53

[14] Romero, P. R., & Karp, P. D. (2004). Using functional and organizational information to improve genome-wide computational prediction of transcription units on pathway-genome databases. Bioinformatics, 20(5), 709-717.

[15] Rudner, D. Z., Fawcett, P., & Losick, R. (1999). A family of membrane-embedded metalloproteases involved in regulated proteolysis of membrane-associated transcription factors. Proceedings of the National Academy of Sciences, 96(26), 14765-14770.

[16] Schroeder, J. W., & Simmons, L. A. (2013). Complete genome sequence of Bacillus subtilis strain PY79. Genome Announc., 1(6), e01085-13.

[17] Travers, M., Paley, S. M., Shrager, J., Holland, T. A., & Karp, P. D. (2013). Groups: knowledge spreadsheets for symbolic biocomputing. Database, 2013.

[18] Youngman, P. J., Perkins, J. B., & Losick, R. (1983). Genetic transposition and insertional mutagenesis in Bacillus subtilis with Streptococcus faecalis transposon Tn917. Proceedings of the National Academy of Sciences, 80(8), 2305-2309.

[19] Wang, X., Le, T. B., Lajoie, B. R., Dekker, J., Laub, M. T., & Rudner, D. Z. (2015). Condensin promotes the juxtaposition of DNA flanking its loading site in Bacillus subtilis. Genes & development, 29(15), 1661-1675.

[20] Wang, X., Brandão, H. B., Le, T. B., Laub, M. T., & Rudner, D. Z. (2017). Bacillus subtilis SMC complexes juxtapose chromosome arms as they travel from origin to terminus. Science, 355(6324), 524-527.

[21] Watson, J. D. et al., Molecular Biology of the Gene (Cold Spring Harbor Laboratory Press, Cold Spring Harbor, New York, ed. 7th, 2014). pp. 205